TKK Dissertations 138
Espoo 2008

EFFECT OF SUPPORT MATERIAL ON THE PERFORMANCE OF CHROMIA DEHYDROGENATION CATALYSTS

Doctoral Dissertation

Satu Korhonen

Helsinki University of Technology
Faculty of Chemistry and Materials Sciences
Department of Biotechnology and Chemical Technology

TKK Dissertations 138
Espoo 2008

EFFECT OF SUPPORT MATERIAL ON THE PERFORMANCE OF CHROMIA DEHYDROGENATION CATALYSTS

Doctoral Dissertation

Satu Korhonen

Dissertation for the degree of Doctor of Science in Technology to be presented with due permission of the Faculty of Chemistry and Materials Sciences for public examination and debate in Auditorium KE2 (Komppa Auditorium) at Helsinki University of Technology (Espoo, Finland) on the 21st of November, 2008, at 12 noon.

Helsinki University of Technology
Faculty of Chemistry and Materials Sciences
Department of Biotechnology and Chemical Technology

Teknillinen korkeakoulu
Kemian ja materiaalitieteiden tiedekunta
Biotekniikan ja kemian tekniikan laitos

Distribution:
Helsinki University of Technology
Faculty of Chemistry and Materials Sciences
Department of Biotechnology and Chemical Technology
P.O. Box 6100
FI - 02015 TKK
FINLAND
URL: http://chemtech.tkk.fi/
Tel. +358-9-451 2616
Fax +358-9-451 2622
E-mail: satu.korhonen@iki.fi

ISBN 978-951-22-9551-7
ISBN 978-951-22-9552-4 (PDF)
ISSN 1795-2239
ISSN 1795-4584 (PDF)
URL: http://lib.tkk.fi/Diss/2008/isbn9789512295524/

TKK-DISS-2506

Multiprint Oy
Espoo 2008

ABSTRACT OF DOCTORAL DISSERTATION	HELSINKI UNIVERSITY OF TECHNOLOGY P.O. BOX 1000, FI-02015 TKK http://www.tkk.fi

Author Satu Korhonen

Name of the dissertation
Effect of support material on the performance of chromia dehydrogenation catalysts

Manuscript submitted May 23, 2008	Manuscript revised September 15, 2008

Date of the defence November 21, 2008

☐ Monograph ☒ Article dissertation (summary + original articles)

Faculty	Faculty of Chemistry and Materials Sciences
Department	Department of Biotechnology and Chemical Technology
Field of research	Industrial Chemistry
Opponent	Professor J.W. Niemantsverdriet
Supervisor	Professor A. Outi I. Krause

Abstract

The effect of support material on the dehydrogenation performance of chromia catalysts was studied with zirconium oxide (zirconia), aluminum oxide (alumina), and zirconia/alumina as the support materials. The dehydrogenation performance of the supports and chromia catalysts was studied by in situ infrared and Raman spectroscopies and activity measurements. The active surface sites of the supports and catalysts were characterized by in situ infrared and Raman spectroscopies using probe molecules, and the surface of zirconia was studied in more depth by modeling with density functional theory (DFT).

The characterization experiments and DFT calculations revealed the amphoteric character of the hydroxyl groups of zirconia and the presence of coordinatively unsaturated (c.u.s.) acid–base pairs. The hydroxyls of alumina exhibited similar basicity to those of zirconia, but their acidity was lower. Lewis acid and Lewis base sites were observed for alumina, but they did not form c.u.s. acid–base pairs as on zirconia. The deposition of zirconia on alumina decreased the Lewis acidity of the c.u.s. sites and the acidity of the hydroxyls, while the total basicity of the material appeared to increase. The addition of chromium also appeared to increase the basicity.

Zirconia was the most active and selective support material in the dehydrogenation of isobutane. The high activity was suggested to originate from the acid–base pairs that were present only on the zirconia surface. The performance of zirconia/alumina resembled that of alumina more than that of zirconia. The benefit of zirconia deposition on alumina was a lower coke deposition rate than on alumina due to the lower Lewis acidity of the zirconia/alumina. However, the cracking activity of alumina was not influenced by zirconia deposition and this was attributed to the presence of similar hydroxyls.

The chromia/zirconia catalyst was the most active dehydrogenation catalyst. The deposition of zirconia on alumina decreased the activity of the chromia catalysts. This was attributed to an incomplete monolayer of zirconia on alumina, which enabled chromium to interact with both zirconia and alumina. In contrast to the supports, the rate of coke deposition was not influenced by the acid–base properties of the catalysts but followed the dehydrogenation activity, and the formation of cracking products was due to thermal cracking. It was concluded that deposition of zirconia on alumina is not beneficial for chromia dehydrogenation catalysts. High surface area zirconias should be investigated instead.

Keywords dehydrogenation, zirconia, alumina, chromia, infrared, Raman, DFT

ISBN (printed) 978-951-22-9551-7	ISSN (printed) 1795-2239
ISBN (pdf) 978-951-22-9552-4	ISSN (pdf) 1795-4584
Language English	Number of pages 72 p. + app. 53 p.

Publisher Helsinki University of Technology, Department of Biotechnology and Chemical Technology

Print distribution Helsinki University of Technology, Department of Biotechnology and Chemical Technology

☒ The dissertation can be read at http://lib.tkk.fi/Diss/2008/isbn9789512295524/

VÄITÖSKIRJAN TIIVISTELMÄ	TEKNILLINEN KORKEAKOULU PL 1000, 02015 TKK http://www.tkk.fi

Tekijä Satu Korhonen

Väitöskirjan nimi
Kantajamateriaalien vaikutus kromioksidi-dehydrauskatalyyttien toimintaan

Käsikirjoituksen päivämäärä 23.5.2008	Korjatun käsikirjoituksen päivämäärä 15.9.2008

Väitöstilaisuuden ajankohta 21.11.2008

☐ Monografia	☒ Yhdistelmäväitöskirja (yhteenveto + erillisartikkelit)

Tiedekunta	Kemian ja materiaalitieteiden tiedekunta
Laitos	Biotekniikan ja kemian tekniikan laitos
Tutkimusala	Teknillinen kemia
Vastaväittäjä	Professori J.W. Niemantsverdriet
Työn valvoja	Professori A. Outi I. Krause

Tiivistelmä

Zirkoniumoksidin (zirkonia), alumiinioksidin (alumina) ja zirkonia/aluminan avulla tutkittiin kantajamateriaalin vaikutusta kromioksidi-dehydrauskatalyyttien toimintaan. In situ infrapuna ja Raman –spektroskopioita ja aktiivisuusmittauksia käytettiin kantajien ja katalyyttien toimintakyvyn määritykseen dehydrausreaktiossa. Kantajien ja katalyyttien aktiivisia pintapaikkoja tutkittiin in situ infrapuna ja Raman –spektroskopioden avulla adsorboimalla näytteille koetinmolekyylejä. Zirkonian pintaa tutkittiin lisäksi mallintamalla tiheysfunktioteorian (DFT) avulla.

Karakterisointikokeiden ja DFT-laskelmien mukaan zirkonian hydroksyyliryhmät olivat amfoteerisiä. Lisäksi zirkonian pinnalla oli happo-emäspareja. Aluminan hydroksyylien emäksisyys oli samansuuruista zirkonian hydroksyylien kanssa, mutta niiden happamuus oli matalampi. Aluminan pinnalla havaittiin Lewis happo- ja Lewis emäspaikkoja, mutta nämä eivät muodostaneet happo-emäspareja. Zirkonian lisäys aluminan pinnalle laski kantajan Lewis happamuutta ja hydroksyylien happamuutta, mutta kantajan kokonaisemäksisyys vaikutti kasvavan. Myös kromioksidin lisäys kasvatti näytteiden emäksisyyttä.

Zirkonia oli aktiivisin ja selektiivisin kantajamateriaali isobutaanin dehydrausreaktiossa. Aktiivisuuden pääteltiin johtuvan happo-emäspareista, joita ei havaittu muilla kantajilla. Zirkonia/alumina käyttäytyi dehydrausolosuhteissa kuten alumina. Koksin muodostuminen oli kuitenkin hitaampaa zirkonia/aluminalla kantajan matalammasta Lewis happamuudesta johtuen. Aluminan ja zirkonia/aluminan samanlaisten krakkausaktiivisuuksien pääteltiin johtuvan samantyyppisistä hydroksyyliryhmistä.

Kromioksidi/zirkoniakatalyytti oli aktiivisin katalyytti dehydrausreaktiossa. Zirkonian lisäys aluminan pinnalle laski kromioksidikatalyyttien aktiivisuutta. Tämän pääteltiin johtuvan vajaasta zirkoniakerroksesta aluminan pinnalla, joka mahdollisti kromin vuorovaikutukset niin zirkonian kuin aluminan kanssa. Koksin muodostumisnopeus kromioksidikatalyyteillä riippui katalyytin dehydrausaktiivisuudesta ja krakkaustuotteet syntyivät termisissä reaktioissa. Johtopäätöksenä todettiin, ettei zirkonian lisäys ollut hyödyllistä kromioksidikatalyyttien toiminalle dehydrausreaktiossa, vaan tutkimuksissa tulisi keskittyä suuren pinta-alan zirkoniakantajiin.

Asiasanat dehydraus, zirkonia, alumina, kromioksidi, infrapuna, Raman, DFT

ISBN (painettu) 978-951-22-9551-7	ISSN (painettu) 1795-2239
ISBN (pdf) 978-951-22-9552-4	ISSN (pdf) 1795-4584
Kieli englanti	Sivumäärä 72 s. + liitteet 53 s.

Julkaisija Teknillinen korkeakoulu, Biotekniikan ja kemian tekniikan laitos

Painetun väitöskirjan jakelu Teknillinen korkeakoulu, Biotekniikan ja kemian tekniikan laitos

☒ Luettavissa verkossa osoitteessa http://lib.tkk.fi/Diss/2008/isbn9789512295524/

PREFACE

The work for this thesis was carried out in the Laboratory of Industrial Chemistry, Helsinki University of Technology, between January 2005 and May 2008; in the Instituto de Catálisis y Petroleoquímica, CSIC, Madrid, Spain, between September and October 2005; and in the Laboratoire de Chimie Théorique, Université P. et M. Curie, Paris, France, in May and between October and December 2007. Funding from the Academy of Finland is gratefully acknowledged. Additional support was received from the European Coordination Action CONCORDE and from the European Science Foundation through COST Action D36. The Finnish Foundation for Technology Promotion (Tekniikan edistämissäätiö) provided a personal grant.

I am most grateful to my supervisor, Professor Outi Krause, for her support, advice, and interest in my studies. Warm thanks are due to my co-authors Dr. Sanna Airaksinen, Dr. Miguel Bañares, and Dr. Monica Calatayud for valuable discussions and help in the research, and to Dr. José Fierro for the XPS measurements. I would like to thank Dr. Sanna Airaksinen for her support during my postgraduate studies and Dr. Miguel Bañares for the opportunity to use the Raman equipment at the Instituto de Catálisis y Petroleoquímica. I am indebted to Dr. Monica Calatayud for facilitating my visit to the Laboratoire de Chimie Théorique and for acquainting me with the theoretical methods.

Dr. Arla Kytökivi, Mr. Sami Juutilainen, Mr. Olli Jylhä, and Ms. Heli Vuori are thanked for the preparation of the catalysts, and Mr. Markus Jönsson and Ms. Susanna Wallenius for experimental assistance. Not least, I am grateful to my colleagues at the Laboratory of Industrial Chemistry for creating a warm and relaxed working atmosphere.

Finally, I would like to thank Juuso for his patience and sense of humor, and my mother and sister for their support and encouragement.

Espoo, May 2008

Satu Korhonen

LIST OF PUBLICATIONS

The thesis is based on the following appended publications, which are referred to in the text by their Roman numerals:

I Korhonen, S. T., Calatayud, M., Krause, A. O. I., Stability of hydroxylated ($\bar{1}11$) and ($\bar{1}01$) surfaces of monoclinic zirconia: A combined study by DFT and infrared spectroscopy, *J. Phys. Chem. C* **112** (2008) 6469–6476. DOI: 10.1021/jp8008546.

II Korhonen, S. T., Calatayud, M., Krause, A. O. I., Structure and stability of formates and carbonates on monoclinic zirconia: A combined study by density functional theory and infrared spectroscopy, *J. Phys. Chem. C* (2008), in press. DOI: 10.1021/jp803353v.

III Korhonen, S. T., Bañares, M. A., Fierro, J. L. G., Krause, A. O. I., Adsorption of methanol as a probe for surface characteristics of zirconia-, alumina-, and zirconia/alumina-supported chromia catalysts, *Catal. Today* **126** (2007) 235–247. DOI: 10.1016/j.cattod.2007.01.008.

IV Korhonen, S. T., Airaksinen, S. M. K., Krause, A. O. I., In situ characterization of carbonaceous deposits formed on chromia/zirconia during isobutane dehydrogenation, *Catal. Today* **112** (2006) 37–39. DOI: 10.1016/j.cattod.2005.11.053.

V Korhonen, S. T., Airaksinen, S. M. K., Bañares, M. A., Krause, A. O. I., Isobutane dehydrogenation on zirconia-, alumina-, and zirconia/alumina-supported chromia catalysts, *Appl. Catal. A* **333** (2007) 30–41. DOI: 10.1016/j.apcata.2007.08.040.

The author's contribution to the appended papers:

I, II She planned the research together with the co-authors, carried out the in situ DRIFTS experiments, and participated in a major way in the theoretical work. She interpreted the results and wrote the manuscripts together with the co-authors.

III She planned the research and carried out or supervised the experiments except for the XPS measurements, interpreted the results, and wrote the manuscript together with the co-authors.

IV She planned the research, carried out the experiments, interpreted the results, and wrote the manuscript together with the co-authors.

V She planned the research together with the co-authors and carried out or supervised the in situ DRIFTS and in situ Raman experiments. She interpreted the results and wrote the manuscript together with the co-authors.

CONTENTS

NOMENCLATURE

Catalysts

*x*CrAl	chromia/alumina catalysts with *x* wt-% of Cr
*x*CrZr	chromia/zirconia catalysts with *x* wt-% of Cr
x(*y*)CrZrAl	chromia/zirconia/alumina catalysts with *x* and *y* wt-% of Cr and Zr, respectively
*y*ZrAl	zirconia/alumina supports with *y* wt-% of Zr

Characterization methods

BET	Brunauer–Emmett–Teller
DRIFT	diffuse reflectance infrared Fourier transform (spectroscopy)
FTIR	Fourier transform infrared (spectroscopy)
GC	gas chromatograph(y)
INAA	instrumental neutron activation analysis
MS	mass spectrometer/spectrometry
UV-Vis	ultraviolet–visible (spectroscopy)
XRF	X-ray fluorescence (spectroscopy)
XPS	X-ray photoelectron spectroscopy
XRD	X-ray (powder) diffraction

Compounds

acac	acetylacetonate (ion), $C_5H_7O_2^-$
alumina	aluminum oxide, Al_2O_3
chromia	chromium oxide, CrO_x
chromates	high oxidation state (Cr^{6+}/Cr^{5+}) chromium oxide species
DME	dimethyl ether, CH_3OCH_3
HCOH	formaldehyde, H_2CO
isobutane	2-methylpropane, i-C_4H_{10}
isobutene	2-methylpropene, i-C_4H_8
MeOH	methanol, CH_3OH

YSZ	yttrium-stabilized zirconium oxide
zirconia	zirconium oxide, ZrO_2

Computational work

DFT	density functional theory
E_{XC}	exchange–correlation energy
LDA	local density approximation (method)
PAW	projector augmented wave (method)
PBE	Perdew–Burke–Ernzerhof (functional)
VASP	Vienna ab initio simulation package

Others

ALD	atomic layer deposition
ALE	atomic layer epitaxy
a.u.	arbitary unit
c.u.s.	coordinatively unsaturated
FCC	fluid catalytic cracking
LPG	liquefied petroleum gas
ODH	oxidative dehydrogenation
TON	turnover number
WHSV	weight hourly space velocity

Symbols

δ	bending mode (infrared spectroscopy)
ρ	electron density
ν_{as}	asymmetric stretch (infrared spectroscopy)
ν_s	symmetric stretch (infrared spectroscopy)
Ψ	wavefunction

1 INTRODUCTION

1.1 Industrial dehydrogenation for the production of light alkenes

Propene and butenes are important intermediates in the production of, e.g., polymers and fuel components. The total world market for propene in 2005 was 67.1 million tonnes [1] and the market in Western Europe in 2006 was 15.6 million tonnes [2], and it is estimated that the demand is growing by approximately 5% per year [1,3]. Altogether 31 million tones of butenes were produced in 1997 [4]. These light alkenes are mainly produced as co-products in fluid catalytic cracking (FCC) and steam cracking of naphtha and liquefied petroleum gas (LPG) [1]. Other production methods for propene are dehydrogenation and methathesis, and dehydrogenation is the second most important production method for butenes. These processes supply approximately 5% of the global market of propene [1] and butenes [4], and in total nearly 7 million tonnes of propene and butenes were produced by dehydrogenation in 2000 [5]. These processes are projected to yield 10% of the global supply of propene by 2010 [1].

Dehydrogenation is of industrial importance because it uses relatively cheap light alkanes as feedstock [6]. Alkane dehydrogenation on chromia/alumina (CrO_x/Al_2O_3) was commercialized in the 1930s and was used during World War II to produce butenes for the production of octane for aviation fuels [5]. During the 1980s chromia/alumina catalysts were taken into use in the Catofin process for the production of propene from propane and isobutene from isobutane [5]. Currently five different process configurations (see Table 1) are in use or under development for catalytic dehydrogenation, relaying on either chromia/alumina, or platinum/alumina catalysts. The main problems in the use of these catalysts are the presence of carcinogenic Cr^{6+} in the chromia catalysts and the sensitivity of the platinum toward sulfur and other deactivating impurities in the feed.

Table 1. Industrial dehydrogenation processes [4,5,7].

	Catofin	Oleflex	STAR [a]	FDB [b]	PDH [c]
developer/ licensor	Süd Chemie, ABB Lummus	UOP	Phillips Petroleum, Uhde	Snamprogetti, Yarsintez	Linde, BASF, Statoil
reactor	parallel adiabatic fixed bed	adiabatic moving bed	tubular reactor	fluidized bed	parallel reactors
operation	cyclic	continuous	cyclic	continuous	cyclic
energy input	regeneration	interstage heating in furnace	reactor in furnace	fuel added during regeneration	regeneration
catalyst	CrO_x/Al_2O_3 with alkaline promoters	$Pt/Sn/Al_2O_3$ with alkaline promoters	Pt/Sn on $MgAl_2O_4$/ $ZnAl_2O_4$	CrO_x/Al_2O_3 with alkaline promoters	formerly CrO_x/Al_2O_3, currently Pt hydrotalcite Mg(Al)O

[a] STAR = steam activated reforming

[b] FDB = fluidized bed dehydrogenation

[c] PDH = propane dehydrogenation technology

Dehydrogenation is an endothermic reaction that requires relatively high temperatures and low pressures. The equilibrium reaction is shown in general form in equation 1.

$$C_nH_{2n+2} \leftrightarrow C_nH_{2n} + H_2 \quad (1)$$

Figure 1 presents the temperature (°C) dependency of equilibrium conversions for ethane, propane, and isobutane under atmospheric pressure [8]. The required temperatures decrease slightly with increasing carbon number and branching of the alkane chain. Industrial processes use temperatures above 550 °C [5,7]. The high process temperatures also favor side-reactions such as thermal cracking and deactivation of the catalysts through coke formation. Hence, in all processes the catalyst undergoes dehydrogenation and regeneration. The industrial processes differ mainly in the means of providing the required heat. The Catofin, FDB, and most likely the PDH processes use the heat formed in the exothermic regeneration phase (coke combustion), whereas the Oleflex and STAR processes heat the reactors in furnaces.

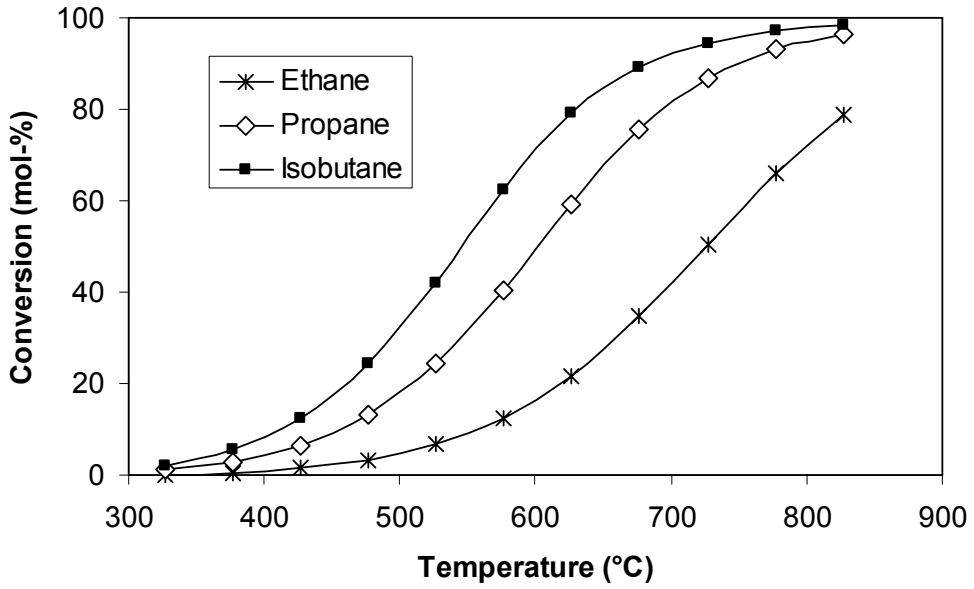

Figure 1. Temperature dependence of the equilibrium conversions for ethane, propane, and isobutane under atmospheric pressure [8].

1.2 Scope of the research

The aim of this work was to study the effect of support material on the performance of chromia dehydrogenation catalysts. Alumina, zirconia (ZrO_2), and zirconia/alumina were chosen as the support materials for the following reasons. Alumina is the conventional industrial support material for chromia dehydrogenation catalysts [4–7], whereas zirconia offers beneficial effects in terms of catalyst activity and selectivity [9]. In addition, zirconia is thermally and chemically more stable than alumina [10]. Nevertheless, zirconia suffers from a low specific surface area in comparison with alumina, and as a potential solution to this problem, it has been deposited on high surface area supports such as alumina [10,11]. Zirconia deposition on alumina was studied, therefore, as a means of combining the beneficial effect of zirconia on the dehydrogenation reaction with the high surface area of alumina.

The main questions of interest were: why zirconia-supported chromia catalysts were more active than the alumina-supported catalysts, and what kind of surface sites were the active centers? In addition, relevant to the topic was: whether the activity of

alumina-supported chromia catalysts could be increased by the deposition of zirconia, and if not, what would be the reasons for this?

Surface-sensitive characterization methods, modeling, and measurements of dehydrogenation activity were chosen as the means to elucidate the effect of support material on the dehydrogenation reaction. The surface of zirconia was studied by density functional theory (DFT) in combination with in situ diffuse reflectance infrared Fourier transform spectroscopy (DRIFTS) [I,II]. The surface and its interaction with water to create hydroxyl groups were modeled, and the theoretical results were confirmed by experiments [I]. The model of the hydroxylated surface was used to study the acid–base properties and the reactive surface sites of monoclinic zirconia by the adsorption of carbon monoxide and carbon dioxide [II]. The formation of carbonaceous surface species was experimentally investigated by in situ DRIFTS [II]. Methanol adsorption–desorption studies [III] were used to characterize the acid–base properties of all supports and catalysts. The formation of carbonaceous surface species was investigated by in situ DRIFT and in situ Raman spectroscopic methods and the formation of gaseous products by mass spectroscopy (MS). The dehydrogenation reaction and the effect of the support material were studied by following the formation of carbonaceous surface species (in situ DRIFTS and in situ Raman spectroscopic methods) during the reaction and by activity measurements [IV,V].

2 DENSITY FUNCTIONAL THEORY

2.1 Theory

The movement of an electron around the nucleus is described by the Schrödinger equation:

$$H\Psi = E\Psi \tag{2}$$

where H is the Hamiltonian (the sum of kinetic and potential energies), Ψ is a wavefunction, and E is the total energy. [12]

Density functional theory (DFT) is based on the correspondence between the electron density of a system and the energy. Within Kohn–Sham DFT the total energy is given as

$$E[\rho] = T_S[\rho] + E_{ne}[\rho] + E_{ee-CL}[\rho] + E_{XC}[\rho] \tag{3}$$

where E is the total energy of the system, ρ is the electron density, T_s is the non-interacting kinetic energy, E_{ne} is the electron–nuclear interaction energy, $E_{ee\text{-}CL}$ is the classical term (i.e., the Coulomb term) of the electron–electron interaction energy, and E_{XC} is the exchange–correlation energy. Equation 3 divides the total energy of a system into two parts: a non-interacting part and a small correction term (E_{XC}) accounting for the interaction of electrons with one another. The benefits of such an approach are that all terms except E_{XC} can be calculated explicitly, and that the E_{XC} term is small in comparison with the others. Hence, small errors in the approximations for the value of E_{XC} will not significantly affect the value of the total energy. A very simple approximation is that the exchange and correlation energies only depend on the density of the electron gas. This is the local density approximation (LDA), which assumes that the density can be treated locally as a uniform electron gas (i.e., the density is a slowly varying function). If, instead, the electron gas is considered non-uniform, the correspondence of the total energy with a real system may be increased. An approximation of this type is the Perdew–Burke–Ernzerhof (PBE) functional. [12,13]

Menconi and Tozer [14] estimated the performance of seven different E_{XC} functionals in the calculation of diatomic bond lengths and harmonic vibrational frequencies. The PBE functional performed well in their study, and the mean absolute errors [(1)] in bond distances and harmonic vibrational frequencies for 45 singlet ground state diatomic molecules were 0.024 Å [(2)] and 21 cm^{-1}, respectively.

2.2 Vienna ab initio simulation package

The PBE functional was used for all the calculations as implemented in the Vienna ab initio simulation package (VASP) code [15–17]. Figure 2 presents the self-consistency cycle used in the VASP code.

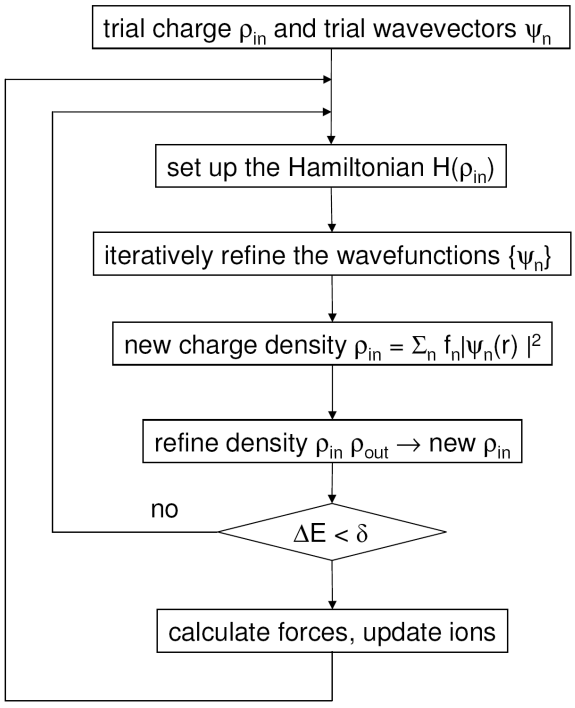

Figure 2. The self-consistency cycle used in the VASP code. Modified from Ref. 18.

---

(1) the mean absolute error: |d| = |calculated - experimental|

(2) 1 Å = 0.1 nm = 10^{-10} m

In this calculation method the Kohn–Sham equation is initially set up with the use of a trial charge (ρ_{in}). The Kohn–Sham equation is then solved to obtain the wavefunctions (Ψ_n) which are used to calculate new charge densities and a new Schrödinger equation. This cycle is iterated until the required accuracy is obtained.

The VASP code uses the projector augmented wave (PAW) method [19−21] to accelerate the calculation speed. In the PAW method the core electrons of an atom are pre-calculated in an atomic environment and kept frozen through the remaining calculation. Therefore, only the outermost and "reactive" electrons are described by the wavefunctions and recalculated in every iteration step.

2.3 DFT in studies on catalysts and catalysis

DFT has been used in studies related to catalysts and catalysis either to describe (i) the adsorption of molecules to surfaces or (ii) the reaction mechanisms of simple catalytic reactions. The adsorption studies are done by placing molecules systematically on different surface sites and by evaluating the stability of the obtained systems in comparison with one another and experimental results [22– 27]. The reaction mechanistic studies can be done either (i) by calculating systematically the activation energies and the transition states of all possible surface processes [28,29], (ii) by using special descriptors that allow the rapid screening of the performance of different surfaces in the same reaction [30] or (iii) by combining the above mentioned methods.

The strength of DFT in studies related to catalysts and catalysis lies in the accuracy and efficiency of the calculation method [30]. The current supercell sizes that can be calculated on high performance computers are between 300 and 400 atoms [24]. The weaknesses of DFT are mainly related to the self-interaction property of the method and the E_{XC} functionals [31]. The self-interaction causes unpaired electrons to become delocalized over many atoms, and if not corrected the model describes, e.g., oxygen vacancies incorrectly [31]. Many E_{XC} functionals tend to overestimate the strength of

the interaction between adsorbing atoms and surfaces [28]. The binding is overestimated by 0.3 eV [(3)] in the PBE [28].

Most of the DFT calculations related to catalysts and catalysis have been performed on metal surfaces [30]. Metal oxides have been less studied in the past mainly due to the need of larger models and, thus, due to the more demanding calculations. The main problem in modeling catalytic surfaces is the inhomogenity of real catalysts and the lack of detailed information on the composition of the surface and the active sites [32,33]. The most recent DFT studies related to catalysts and catalysis are striving toward realistic surface models and models that would be able to predict new active catalysts. The correspondence between the surface model and a real catalyst can be improved by taking into account the reaction condition. The effect of temperature and pressure (DFT calculations are carried out at 0 K [(4)]) on the stability of surfaces and surface species can be estimated by statistical thermodynamic analysis [22–27]. Such studies have, e.g., shown that the degree of hydroxylation influences the acid–base properties of γ-alumina and the properties of alumina-supported palladium particles [23,24]. Specific descriptors have enabled the prediction of new catalytically active surfaces. The use of nitrogen adsorption energy on metal surfaces as a descriptor for the catalytic activity in ammonia synthesis predicted an alloy of cobalt and molybdenum to be more active than the industrially used iron [30]. This was later verified by experiments [30].

In this study DFT was used to study the surface of monoclinic zirconia, its interaction with water to create hydroxyl groups, and its acid–base properties. Statistical thermodynamic analysis was applied to study the effect of temperature and pressure on the degree of hydroxylation. The formation of carbonaceous surface species was studied to evaluate the acid–base properties.

[(3)] 1 eV~ 96.5 kJ/mol

[(4)] 0 K = -273.15 °C

3 CHROMIA-CONTAINING DEHYDROGENATION CATALYSTS

Chromia/alumina (CrO_x/Al_2O_3) catalysts are widely used in industry for the dehydrogenation reaction. The system has been extensively studied during the past decades [4–6,9,34– 39]. The activity of chromia dehydrogenation catalysts can be enhanced, e.g., by adding alkali dopants [39] or through the use of zirconia (ZrO_2) rather than alumina as support material [9]. The drawback of zirconia is that its specific surface area is much lower than that of alumina. As a means of overcoming this problem, zirconia has been deposited on high surface area oxides such as alumina [10,11,40– 43], either by impregnation from solution [10,40–43] or by atomic layer deposition (ALD) (previously know as atomic layer epitaxy, ALE) [11]. In the ALD technique the deposition occurs through self-terminating and saturating gas–solid reactions, which ensure a high dispersion and homogeneity of the material [11,44].

3.1 Characteristics of zirconia, alumina, and zirconia/alumina

Pure, bulk zirconia exhibits three well-defined crystal phases, of which the monoclinic phase (stable below ~1100 °C [45]) is commonly used for catalytic applications. With increasing temperature the monoclinic phase transforms into tetragonal (stable below ~2400 °C) and cubic (stable below the melting point of ~2670 °C) phases [45]. Zirconia can be stabilized in the tetragonal or cubic phases at ambient temperatures by doping with, e.g., yttrium (yttrium-stabilized zirconia, i.e., YSZ), or in the tetragonal phase by reducing the particle size to nano-scale (below ~30 nm) [45]. In the bulk of the monoclinic phase the zirconium atoms are seven-fold coordinated, whereas in the bulk of the tetragonal and cubic structures the coordination is eight-fold [46]. The bulk coordination of oxygen atoms is three- and four-fold in monoclinic zirconia and four-fold in the tetragonal and cubic phases. The most stable surfaces for monoclinic, tetragonal, and cubic zirconia are ($\bar{1}11$) [47], (101) [48], and (111) [47], respectively.

The surface species on zirconia are different hydroxyl groups, coordinatively unsaturated (c.u.s.) Zr^{4+} and c.u.s. O^{2-} species, and defects such as oxygen vacancies [45,49,50]. The relative concentration of these species depends on the phase of

zirconia, the particle size, the preparation route (e.g., impurities), and the external conditions (e.g., temperature and gas phase composition). The hydroxyl groups on zirconia are amphoteric in character, whereas the c.u.s. Zr^{4+} and c.u.s. O^{2-} sites are Lewis acid and Lewis base sites, respectively [49,50]. Figure 3 presents the different hydroxyl groups and their infrared band positions. On the monoclinic zirconia the hydroxyl groups are mainly terminal and tribridged [49], whereas on the tetragonal zirconia they are predominately bibridged [50]. The amorphous zirconia has roughly equal concentrations of terminal, bibridged, and tribridged hydroxyls [50]. The intensity of the hydrogen-bonded hydroxyls depends on the atmosphere, i.e., the amount of moisture that can adsorb on the surface. The higher acidity of monoclinic than of tetragonal zirconia is mainly due to the higher concentration of hydroxyl groups on the monoclinic surface [50]. The c.u.s. sites form Lewis acid–base pairs (Zr^{4+}–O^{2-}) [49,50], which have stronger acid–base character on the monoclinic than on the tetragonal phase [50].

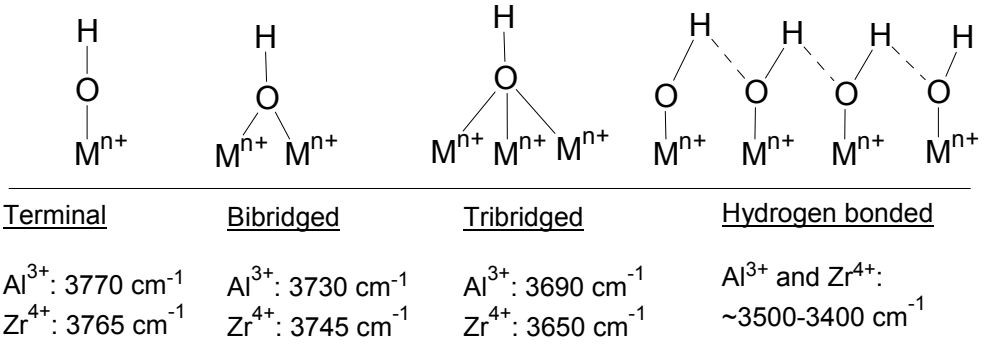

Figure 3. Hydroxyl species on zirconia and alumina, and positions of their infrared bands. [50,51]

Seven polymorphs of alumina exist, of which the γ-, η-, δ-, and θ-Al_2O_3 are typically used in catalytic processes [45]. The phase transformation occurs with increasing temperature in the presented order, but the exact temperatures depend on the hydroxide precursor (e.g., bayerite or gibbsite). The four mentioned phases are meta-stable in the range of ~470–1100 °C. The phases can further be divided into low-temperature (γ- and η-Al_2O_3) and high-temperature (δ- and θ-Al_2O_3) phases, of which the low-temperature ones are catalytically more active. All transitional aluminas have a cubic crystal structure, and the structural differences between the different phases are minor. For particles of γ-alumina the (110) surface predominates, and there are minor fractions of

(100) and (111) surfaces [23]. The surface species on alumina are different hydroxyl groups (terminal, bibridged, tribridged, and hydrogen-bonded; see Figure 3) and c.u.s. Al^{3+} and c.u.s. O^{2-} species. The surface basicity of alumina is low, and the material is catalytically important due to its acidic properties. The acidity of the hydroxyl groups increases with decreasing band position, i.e., the terminal hydroxyls are basic, and the acidity increases from the bibridged to the tribridged hydroxyls. [51]

The structure of zirconia on alumina depends on the surface density of zirconium on the support. The monolayer capacity of zirconia on alumina (calculated on the basis of the specific surface area of the support) has been estimated to be 4–5 at_{Zr}/nm^2 [11] or even 7.4 at_{Zr}/nm^2 [41]. Below the monolayer coverage zirconia is amorphous, whereas at higher loadings it forms nano-sized tetragonal or cubic zirconia crystallites, or islands of these [10,11,43]. Owing to the formation of the zirconia crystallites, however, it has been suggested that even a surface density of 7.5 at_{Zr}/nm^2 is unable fully to cover the surface [43]. Especially at low loadings, zirconia may also migrate into the alumina matrix forming a mixed oxide [10,40,41]. Damyanova et al. [10] and Kytökivi et al. [11] have reported that the hydroxyls on zirconia/alumina do not resemble those on zirconia even at zirconia loadings near the monolayer coverage. Measurements of pyridine adsorption on zirconia/alumina have shown that the deposition of zirconia reduces the concentration of strong Lewis acid sites while increasing that of the weak Lewis acid sites [10].

3.2 Supported chromia catalysts

The possible oxidation states of chromium on inorganic oxides are +2, +3, +5, and +6, but their occurrence depends on the support material, catalyst preparation and pretreatment conditions, and the chromium content [34]. The monolayer coverage of chromium on alumina is approximately 4–5 at_{Cr}/nm^2 [6,35,36] calculated on the basis of the specific surface area of the support. The monolayer coverage on zirconia has been estimated to be 5 at_{Cr}/nm^2 [9] or even 9 at_{Cr}/nm^2 [35] (calculated on the basis of the specific surface area of the support).

3.2.1 Oxidized chromia catalysts

Under oxidizing conditions at low surface densities of chromium (up to ~0.5 at_{Cr}/nm^2) the main species on alumina are Cr^{6+}, but traces of Cr^{5+} (1–2% of total chromium [9]) are also present, and the chromium species are mainly monochromates [6]. On zirconia, in turn, similar amounts of Cr^{5+} (50% of total chromium) and Cr^{6+} are present at low surface densities (up to ~0.8 at_{Cr}/nm^2) [9]. At intermediate coverage, Cr^{3+} species appear, and the fraction of polychromates increases with the coverage [6,9]. Above the monolayer coverage, on both oxides, crystalline α-Cr_2O_3 is formed and the main oxidation state is +3 [6,9].

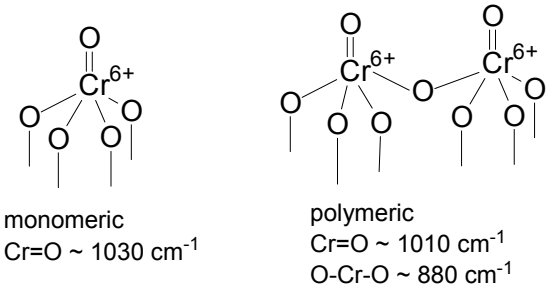

Figure 4. Monomeric and polymeric Cr^{6+} species and their Raman and infrared Cr–O vibrational frequencies. [35,52]

Figure 4 presents a schematic drawing of the molecular structures of monomeric (monochromates) and polymeric (polychromates) Cr^{6+} species and their approximate Raman and infrared Cr–O vibrational frequencies. The band positions are support dependent, e.g., ~1030 cm^{-1} for chromia/zirconia and ~1020 cm^{-1} for chromia/alumina [35,52]. In addition to the bands of the Cr^{6+} species, infrared measurements of calcined chromia/zirconia may show Cr^{5+}=O vibrations [53] at 1018 and 1004 cm^{-1}. Raman and infrared spectroscopies do not typically show metal–O–support bonds [54,55].

3.2.2 Reduced chromia catalysts

On alumina, the high oxidation state species are reduced in the presence of alkanes, hydrogen, and carbon monoxide to produce Cr^{3+} and possibly some Cr^{2+} [4,6,37,38]. The Cr^{2+} species are more common on carbon monoxide reduced silica-supported

(SiO_2) catalysts [56]. On zirconia, the Cr^{6+} and Cr^{5+} species are reduced under carbon monoxide to Cr^{2+} and Cr^{3+} species, respectively [9]. The active sites for dehydrogenation are the Cr^{3+} species [4–6,9,34–39]. De Rossi et al. [9] assigned the higher dehydrogenation activity of chromia/zirconia than of chromia/alumina to the high concentration of monomeric Cr^{5+} species, which are reduced under the reaction conditions to monomeric Cr^{3+} species. Hakuli et al. [38] reported for chromia/alumina that the dehydrogenation activity is insensitive both to the size of the Cr^{3+} species and to their redox history.

4 EXPERIMENTAL

The experimental procedures are described in detail in papers I–V. Only a short summary is given here.

4.1 Computational work

The PBE functional was used for all the calculations as implemented in the VASP code [15–17]. The electron configurations [Kr]$4d^2 5s^2$, [He]$2s^2 2p^4$, and [He]$2s^2 2p^2$ were used for zirconium, oxygen, and carbon atoms, respectively. The core electrons are presented in square brackets. These were kept frozen and replaced by PAW-generated pseudopotentials [20,21], while the valence electrons were described with a plane wave basis set with cutoff of 400 eV. The distance between k-points in the reciprocal space was 0.05 $Å^{-1}$.

The most stable ($\bar{1}11$) and ($\bar{1}01$) surfaces [47] of the monoclinic zirconia were chosen for the calculations. A slab containing four ZrO_2 layers was selected for the ($\bar{1}11$) surface (see Figure 7, p. 41), and this was repeated periodically in three dimensions. The (1×1) unit cell dimensions for the ($\bar{1}11$) surface were 7.446×6.793 $Å^2$, and the slab contained four ZrO_2 units per layer (total of 48 atoms). A (2×1) unit cell was chosen for the ($\bar{1}01$) surface to keep the number of surface zirconium atoms constant for the different surfaces. Owing to the larger size of the unit cell, a two-layer slab was used for this surface (also a total of 48 atoms). The unit cell dimensions were 8.618×8.340 $Å^2$. The adsorption studies were performed on one side of a slab, and the full model was allowed to relax with the conjugate algorithm until the difference in the energy was less than 0.001 eV. A vacuum of 10 Å prevented the interaction between successive slabs.

The vibrational frequencies of the model systems were calculated by finite differences within the harmonic approximation. The Hessian matrix was then constructed and diagonalized. Scaling factors [57,58] and correction terms [59] have sometimes been used to account for the anharmonicity of vibrations. However, in this study no such corrections were made to the obtained vibrational frequencies.

To estimate the accuracy of the chosen calculation method, the vibrational frequencies for gaseous water, carbon monoxide, and carbon dioxide were calculated [unpublished results]. These frequencies are compared with experimental ones [60] in Table 2. The errors in the vibrational frequencies for gaseous carbon monoxide and carbon dioxide are small. However, the calculations are unable to produce combination modes and overtones. Thus, the calculations are also unable to produce the experimentally observed Fermi resonance for carbon dioxide. The errors in the vibrational frequencies for water are larger than for carbon monoxide and carbon dioxide, and the calculations tend to overestimate the frequencies. The large error for water is due to the high anharmonicity of the O–H bonds [22]. To estimate the validity of the model systems, the calculated vibrational frequencies were compared with those observed by infrared spectroscopy for commercial monoclinic zirconia under different atmospheres.

Table 2. The experimental (exp.) [60] and calculated (calc.) [unpublished results] vibrational frequencies (cm^{-1}) for gaseous water, carbon monoxide, and carbon dioxide.

	H_2O			CO			CO_2		
	exp.	calc.	error [a]	exp.	calc.	error [a]	exp.	calc.	error [a]
ν_{as}	3756	3821	65	2134 [b]	2132 [b]	-2	2349	2364	15
ν_s	3657	3738	81				1285/1388 [c]	1348	---
δ	1595	1601	6	---	---	---	667	665	-2

[a] error = calculated - experimental

[b] Two atom molecule, the stretch is neither asymmetric nor symmetric

[c] Fermi resonance

4.1.1 Hydrated surfaces

The adsorption of water on the zirconia surfaces [I] was studied to elucidate the formation of hydroxyl groups, and to create a model surface that could be considered realistic under actual catalytic reaction conditions. The adsorption of one to four water molecules per unit cell was studied. Since each unit cell contained four zirconium atoms, this corresponded to a coverage of $\theta = 0.25–1$. Both dissociative and molecular adsorptions of water at all coverage were considered.

The stability of the hydrated surfaces was studied in respect to both temperature and water vapor pressure by statistical thermodynamic analysis. This method has been previously applied to other hydroxylated metal oxide surfaces [22–27]. The formalism assumes a thermodynamic equilibrium between the gas phase water and the surface. The analysis was performed as follows: (i) the surface free energies of a series of model surfaces were calculated by total energy calculations, (ii) the energies as a function of the chemical potential of water were used to draw a phase diagram, and (iii) the chemical potentials were related to the temperature and water partial pressure.

4.1.2 Structure and stability of formates and (bi)carbonates

The structure and stability of formates and (bi)carbonates [II] were studied to gain a deeper insight into the active surface species and the acid–base properties of monoclinic zirconia. These studies were performed for the ($\bar{1}11$) zirconia surface containing one dissociatively adsorbed water molecule (see Figure 8, p. 42). The formate and (bi)carbonates were considered to form by insertion of carbon monoxide and carbon dioxide, respectively, into a hydroxyl group. Both terminal and bibridged hydroxyl groups were considered for the formation. The adsorption of carbon monoxide and carbon dioxide was also studied on the c.u.s surface atoms.

4.2 Preparation of supports and catalysts

Table 3 (p. 37) presents the studied supports and catalysts. The catalysts will be referred to as *x*(*y*)CrZ, where *x* is the amount of chromium in wt-%, *y* is the amount of zirconium on the zirconia/alumina supports in wt-%, and *Z* is the support (Zr for zirconia, Al for alumina, and ZrAl for zirconia/alumina). The support materials were commercial zirconia (Mel Chemicals EC 0100 1/8 in) [I–V] and alumina (Akzo 000-1.5 E) [III,V], and ALD-prepared zirconia/alumina [III,V]. All supports were calcined in air at 600 °C for 16 h.

In the ALD method, the zirconia deposition was performed at elevated temperature with sequences of zirconium precursor ($ZrCl_4$, Fluka 98%) deposition and water vapor flush

(to decompose the complex). Two zirconia/alumina supports, prepared using one and five sequences of precursor deposition and water vapor flush, were used in the studies. The deposition of zirconia on alumina is described in detail elsewhere [11].

Chromia was deposited on the supports by an ALD method [III–V] similar to that used for zirconia deposition, and is described in detail elsewhere [38]. The precursor for chromium deposition was chromium acetylacetonate ($Cr(acac)_3$, Riedel-de Haën 99%). The chromium complexes were decomposed with air at elevated temperatures. One or two sequences of chromium deposition and complex decomposition were applied. One chromia/zirconia sample (2.7CrZr [IV]) was also prepared by incipient wetness impregnation with $Cr(NO_3)_3 \cdot 9H_2O$ (Aldrich 99%) as the precursor. This was done to create a sample with higher chromium loading. All chromia catalysts were calcined in air at 600 °C for 4 h.

4.3 Characterization by BET, XRF, XRD, XPS, and UV-Vis

The surface area and porosity of the samples were determined by Brunauer–Emmett–Teller (BET) method. X-ray diffraction (XRD) was used to determine the phase of the commercial zirconia. The elemental composition of the chromia catalysts and the zirconia/alumina supports was determined by X-ray fluorescence (XRF). The chromium content of selected catalysts was determined by instrumental neutron activation analysis (INAA) [unpublished results]. The surface concentrations (at/nm^2) of chromium and zirconium on the samples were calculated with use of the XRF results and the specific surface areas of the supports (BET).

The amount of Cr^{6+} on the calcined catalysts was determined by X-ray photoelectron spectroscopy (XPS) [III], and by UV-Vis spectrophotometry (UV-Shimadzu, λ=375 nm) [V] after dissolution of Cr^{6+} with aqueous sodium hydroxide. The UV-Vis method is described in detail by Haukka [61]. XPS was also used to study the surface composition of the zirconia/alumina support and the zirconia/alumina-supported catalysts [III].

4.4 In situ DRIFTS measurements

The formation of surface species under different atmospheres and temperatures was studied by in situ diffuse reflectance Fourier transform spectroscopy (DRIFTS). In situ DRIFTS is useful for characterizing catalysts and monitoring the formation of surface species under reaction conditions. The equipment consisted of a Nicolet Nexus Fourier transform infrared (FTIR) spectrometer equipped with a Spectra-Tech high temperature and high pressure reaction chamber. The gaseous products were analyzed on-line with a Pfeiffer Vacuum Omnistar mass spectrometer (MS).

The catalysts were studied undiluted in powder form. All samples were calcined in situ with 10% oxygen in nitrogen at 580 °C for 2 h and reoxidized at the same temperature after the experiments with 2–10% oxygen in nitrogen for 30 min. In all experiments the spectrum measured with an aluminum mirror (4 cm^{-1}, 200 scans) was used as the background, and the total gas flow was kept constant at 50 cm^3/min. All gases except carbon monoxide (Messer Griesheim GmbH, 99.997%) were from AGA (carbon dioxide 99.99%, hydrogen 99.999%, isobutane 99.95%, nitrogen 99.999%, synthetic air 99.99%, and 2000 ppm methanol in nitrogen mixture). In addition, the nitrogen gas was purified with Oxisorb (Messer Griesheim GmbH).

4.4.1 Measurements of carbon dioxide and carbon monoxide adsorption

The adsorption of carbon dioxide and carbon monoxide was performed to study the acid–base properties the zirconia, alumina, and 4.4ZrAl supports. The vibrational frequencies of the formate and (bi)carbonate species on monoclinic zirconia were compared with those obtained by computational methods.

Measurements of the adsorption of carbon dioxide on the zirconia [II], alumina [unpublished results], and 4.4ZrAl [unpublished results] supports were done to study the basic properties of the supports. Carbon dioxide adsorbs on the basic sites of metal oxides forming different surface species according to the type of surface site. Figure 5 presents the different carbonate species detected by Bachiller-Baeza et al. [49] for monoclinic and tetragonal zirconia. The bicarbonate species, sometimes also referred to

as hydrogen carbonate species, are formed in a reaction between the basic, terminal hydroxyl groups and carbon dioxide. The bidentate carbonate species are formed on an acid–base pair (e.g., c.u.s. Zr^{4+}–O^{2-}) and the monodentate species on highly basic c.u.s. O^{2-} sites. Polydentate species are formed on surfaces with closely spaced c.u.s Zr^{4+} sites.

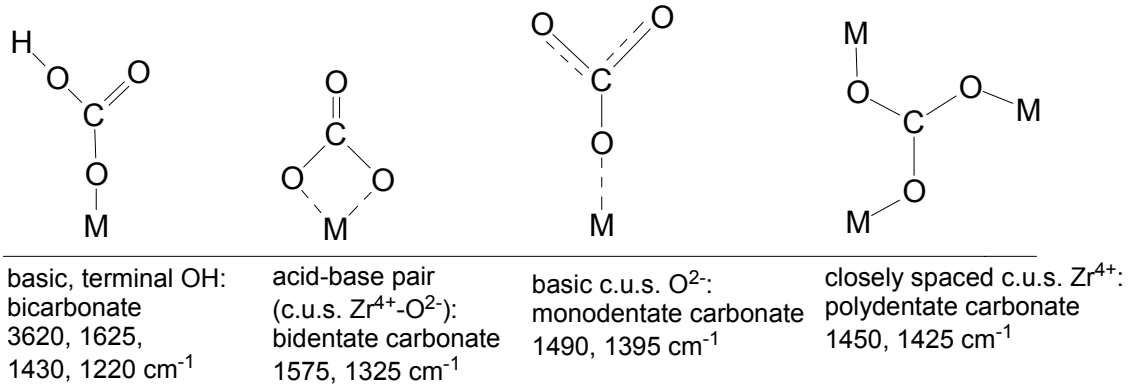

Figure 5. Possible carbonate species formed during carbon dioxide adsorption. Infrared bands reported by Bachiller-Baeza et al. [49] for monoclinic and tetragonal zirconia.

The measurements were done by directing 5% carbon dioxide in nitrogen to the calcined sample at 30 °C for 5 min, after which the sample was flushed with nitrogen at the same temperature for 30 min. The spectra were recorded under carbon dioxide once every minute (4 cm^{-1}, 30 scans), and during the nitrogen flush once every minute (4 cm^{-1}, 30 scans) for the first 5 min and thereafter once every 5 min (4 cm^{-1}, 100 scans). Thereafter the sample was slowly heated in nitrogen to 100 °C and the spectra were recorded at 50, 75, and 100 °C (4 cm^{-1}, 100 scans) under nitrogen. At 100 °C the carbon dioxide adsorption was repeated by directing the 5% carbon dioxide in nitrogen flow to the sample for 5 min and then flushing with nitrogen for 15 min. The spectra were recorded as at room temperature. The experiment was continued by heating and measuring of the spectra under nitrogen every 25 °C. Carbon dioxide was directed to the sample at 30, 100, 200, 300, 400, 500, and 580 °C for 5 min followed by a 15 min nitrogen flush. The gaseous products were monitored on-line by MS.

Measurements of the adsorption of carbon monoxide on the zirconia [II], alumina [unpublished results], and 4.4ZrAl [unpublished results] supports were done to study the acidic properties of the supports. Formates are formed in a reaction between the basic

gaseous carbon monoxide and the hydroxyl groups [62]. The measurements were done by heating the sample under 5% carbon monoxide in nitrogen from 30 to 100 °C during which spectra were recorded at 30, 50, 75, and 100 °C (4 cm^{-1}, 100 scans). At 100 °C the sample was flushed with nitrogen for 5 min, after which a spectrum (4 cm^{-1}, 100 scans) was recorded. Thereafter the carbon monoxide-containing flow was redirected to the sample and the heating was continued. The spectra were recorded under carbon monoxide every 25 °C up to 580 °C and during nitrogen flushing at 100, 200, 300, 400, 500, and 580 °C. The gaseous products were monitored on-line by MS.

4.4.2 Measurements of methanol adsorption–desorption

Adsorption and desorption of methanol on the zirconia, alumina, and 4.4ZrAl supports and on the chromia catalysts were measured to study the acid–base properties and the composition of the functional surface species on the supports and catalysts [III]. Measurements of methanol adsorption give information on the surface composition (chemisorbed methanol, i.e., methoxy species) and on the chemical character of the surface species (reaction products). Adsorption of a monolayer of methanol on the catalyst surface and the application of vibrational spectroscopic techniques (DRIFTS and Raman) allows the surface to be characterized from the specific vibrations of the formed methoxy species. Furthermore, the functional surface species can be identified by monitoring (MS) the gaseous products. The conditions for methanol adsorption were chosen according to Briand et al. [63], who report that the use of dilute methanol feed (2000 ppm) at 100 °C is optimal for the formation of a monolayer of chemisorbed methanol. According to Wang and Wachs [64], the formation of carbon dioxide, formaldehyde (HCOH), and dimethyl ether (DME) is indicative of the presence of basic, redox, and Lewis acid surface sites, respectively.

The measurements were performed either as (i) an adsorption at 100 °C followed by heating in nitrogen up to 580 °C (adsorption–desorption) or as (ii) a temperature-dependent measurement, in which the samples were heated slowly in 2000 ppm methanol in nitrogen flow from room temperature to 580 °C. The adsorption–desorption experiments were performed to study the chemisorption of methanol, whereas the

temperature-dependent measurements were performed to further study the reactions of the surface species. The gaseous products formed during the temperature-dependent experiments were monitored on-line by MS.

4.4.3 Measurements with isobutane

The measurements with isobutane were performed to study the formation of carbonaceous surface species during the dehydrogenation reaction [IV,V]. The experiments were done either as (i) temperature-dependent studies, where the supports and catalysts were heated slowly in 5% isobutane in nitrogen from room temperature to 580 °C, or as (ii) time-dependent studies, where the dehydrogenation reaction was studied at the constant temperature of 580 °C under 5% isobutane in nitrogen. The effect of hydrogen prereduction on the dehydrogenation reaction was studied with both temperature- and time-dependent measurements after reduction of the samples with 5% hydrogen in nitrogen for 15 min at 580 °C. The gaseous products were monitored on-line by MS during the isobutane experiments.

4.5 In situ Raman spectroscopic measurements

Raman spectroscopy was used to characterize the calcined supports and catalysts, and to study the methanol adsorption–desorption reaction and the formation of carbonaceous surface species during the dehydrogenation [III,V]. The in situ Raman–MS measurements were performed with a Renishaw Micro-Raman System-1000 using a home-made quartz flow-through reactor (operando reactor [65]) and an MS for on-line product analysis. The Raman spectrometer consisted of an Ar^+ (514 nm) laser, cooled CCD detector, and a holographic super-notch filter for the removal of elastic scattering. The catalyst sample was loaded to the reactor between two layers of silicon carbide (SiC) to minimize the void volume inside the reactor. The catalyst samples were calcined using 5% oxygen in helium at 570 °C for 2 h, and reoxidized using the same feed at the same temperature for 30 min after the experiments.

4.5.1 Measurements of methanol adsorption–desorption

Measurements of methanol adsorption–desorption [III] were performed by the in situ Raman–MS technique to further study the surface composition and functional surface species on the chromia catalysts. After the calcination and before the methanol adsorption–desorption experiments, the reactor was flushed with helium for 1 h. The methanol adsorption experiments were performed by adsorbing methanol (2000 ppm in helium) at 100 °C. After the adsorption the reactor was flushed with helium and heated stepwise to 350 °C.

4.5.2 Measurements with isobutane

In situ Raman–MS measurements were performed to study the formation of carbonaceous surface species from isobutane on the chromia catalysts at a constant temperature of 570 °C [V]. After the calcination and before the dehydrogenation experiments, the reactor was flushed with helium for 30 min. The dehydrogenation measurements were performed at 570 °C by feeding 5% isobutane in nitrogen to the sample. The spectra were recorded after 2, 12, 22, and 32 min on stream.

4.6 Measurements of dehydrogenation activity

Activities of the supports and catalysts in isobutane dehydrogenation were measured in a continuous flow reaction system consisting of a fixed-bed microreactor and of a Fourier transform infrared (FTIR) gas analyzer and a gas chromatograph (GC) for on-line product analysis [V]. The gases were those used in the in situ DRIFTS measurements (see sect. 4.4, p. 31).

Activities were measured at 560 °C under atmospheric pressure. The samples (0.1 g) were loaded in the reactor between two layers of silicon carbide and heated to the reaction temperature under 5% oxygen in nitrogen. Dehydrogenation was carried out for 15 min by using isobutane feed with a weight hourly space velocity (WHSV) of 15 h^{-1} and diluted with nitrogen at a molar ratio of 3:7. The reaction products were monitored by FTIR for the first 6 min on stream, a GC sample was taken after 10 min, and the

FTIR analysis was continued. After the dehydrogenation, the catalyst was regenerated with diluted air. The regeneration products—carbon oxides and water—were analyzed by FTIR. The amount of coke (as carbon) deposited on the catalyst during dehydrogenation was calculated from the measured amounts of carbon oxides. The hydrogen content of the coke was determined from the amount of water released during the regeneration. In selected experiments the catalyst was prereduced with 10% hydrogen in nitrogen before the dehydrogenation. Water formed in the prereduction was measured by FTIR. Thermal reactions in the system were investigated by replacing the catalyst with inert silicon carbide.

5 RESULTS AND DISCUSSION

5.1 Characterization of the supports and catalysts

5.1.1 Composition of the supports and catalysts

Table 3 presents the supports and catalysts that were studied and their properties as determined by BET, XRF, and UV-Vis techniques.

Table 3. Supports and catalysts and their properties [I–V].

sample	paper	SA (m^2/g)	wt-% Cr	at_{Cr}/nm^2	at_{Cr}^{6+}/nm^2	wt-% Zr	at_{Zr}/nm^2
Al_2O_3 (com.) [a]	III,V	185	---	---	---	---	---
ZrO_2 (com.) [a]	I-V	47	---	---	---	n.a. [b]	n.a. [b]
4.4ZrAl	III,V	165	---	---	---	4.4	1.7
15ZrAl	ref. 11	150	---	---	---	15	5.2
0.4CrZr	III,IV	47	0.4	1.0	0.5	n.a. [b]	n.a. [b]
0.8CrZr	III-V	48	0.8	1.9	1.1	n.a. [b]	n.a. [b]
2.7CrZr (imp.) [c]	IV	45	2.7	6.8	2.1	n.a. [b]	n.a. [b]
1.2CrAl	III	189	1.2	0.7	0.6	---	---
2.2CrAl	V	181	2.2	1.4	1.1	---	---
2.0(4.4)CrZrAl	III,V	169	2.0	1.4	0.8	4.4	1.7
2.1(15)CrZrAl	III,V	148	2.1	1.6	1.2	15	5.2

[a] com. = commercial

[b] n.a. = not analyzed

[c] imp. = impregnated

All supports and catalysts except the commercial zirconia and alumina supports and the 2.7CrZr catalyst were prepared by ALD. According to XRD measurement the

commercial zirconia was mainly in the monoclinic phase, and according to the supplier the commercial alumina was γ-Al_2O_3.

The specific surface areas of the zirconia/alumina supports were of the same order of magnitude as the surface area of alumina, whereas the specific surface area of zirconia was one-third of that. The surface densities of zirconia on alumina were below the monolayer coverage (4–5 at_{Zr}/nm^2 [11]) for 4.4ZrAl and approximately equal to the monolayer coverage for 15ZrAl. The binding energies detected by XPS [III] for the Al 2p and Zr $3d_{5/2}$ photoelectrons were in accordance with values for bulk alumina and zirconia [10,40], irrespective of the studied catalyst or support, suggesting that no mixed oxide was formed during the deposition of zirconia on alumina.

The surface areas of the catalysts were only slightly affected by chromia deposition, and the surface densities of chromium depended on the number of ALD deposition cycles rather than on the support material. The surface density of chromium for all ALD-prepared chromia catalysts was below the monolayer coverage of ~4–5 at_{Cr}/nm^2 [6,35,36], whereas the surface density for the impregnated 2.7CrZr catalyst was above this value. INAA measurements confirmed the XRF results on the chromium content of the catalysts [unpublished results]. The surface density of Cr^{6+} on the calcined catalysts was determined by the UV-Vis technique [V] and by XPS [III]. For the ALD-prepared calcined catalysts, a higher fraction of chromium was in oxidation state +6 than in the oxidation state +3. Repeated UV-Vis measurements on selected catalysts that were reoxidized and releached after the first UV-Vis measurement gave similar surface densities for the Cr^{6+} species: 1.0, 0.8, and 0.9 at_{Cr}^{6+}/nm^2 for the 0.8CrZr, the 2.2CrAl, and the 2.1(15)CrZrAl, respectively [unpublished results]. The results suggested that the observed Cr^{6+} surface densities were equilibrium values dependent on the support material. However, the UV-Vis technique for the quantification of Cr^{6+} species is more accurate for the chromia/alumina catalysts than for the chromia/zirconia catalysts owing to the higher fraction of Cr^{5+} species present on the zirconia support [9]. The Cr^{5+} species are unstable in aqueous solutions and tend to disproportionate ($3Cr^{5+} \rightarrow 2Cr^{6+}+Cr^{3+}$) to soluble Cr^{6+} and finely dispersed, surface-bound Cr^{3+} hydroxide [9]. It was suggested [V] on the basis of the dehydrogenation results that the oxidation state distribution of the chromia species on zirconia/alumina-supported catalysts

resembles that of the alumina-supported catalyst more than that of the zirconia-supported one. However, the XPS [III] results suggested that chromium might preferentially cover zirconia rather than alumina on the zirconia/alumina-supported catalyst.

5.1.2 Surface characteristics of the supports and catalysts

Figure 6A presents the DRIFT spectra of the supports in the hydroxyl stretching region and Figure 6B selected Raman spectra for the chromia catalysts. In accordance with the XRD measurement, the infrared and Raman measurements indicated that the commercial zirconia was monoclinic [III,IV]. And in accordance with the results by Damyanova et al. [10] and Kytökivi et al. [11], the hydroxyl groups of the zirconia/alumina resembled those of alumina rather than those of zirconia [III]. No crystalline zirconia was observed for the zirconia/alumina-supported catalysts in the Raman measurements even after subtraction of the spectrum of the quartz window [III]. This indicated that the deposited zirconia was amorphous, since even microcrystallites (<4 nm [54]) can be detected by Raman spectroscopy if they are present. Microcrystallites are too small to be visible in XRD, i.e., they appear as amorphous.

For all catalysts the intensity of the hydroxyl groups decreased with increasing chromium loading, and the terminal hydroxyl groups were most affected [III]. The band position of the terminal hydroxyl species observed for the zirconia/alumina-supported chromia catalysts was shifted from that observed for the alumina and 4.4ZrAl supports. This was suggested to originate either from the presence of zirconium-bound hydroxyls, in accordance with Kytökivi et al. [11], or from terminal hydroxyls of alumina, with the band shifted due to the presence of chromium. The appearance of zirconium-bound hydroxyls on the zirconia/alumina-supported chromia catalyst would suggest, contrary to the XPS results [III], that chromium preferentially covers alumina rather than zirconia on the zirconia/alumina support, whereas the presence of aluminum-bound hydroxyls would support the XPS results.

The Raman measurements showed that the chromium species were polymeric for all catalysts, and no α-Cr_2O_3 (characteristic Raman band at 550 cm^{-1} [66]) was observed

even for the 2.7CrZr catalyst [III, unpublished data]. Two different polymeric chromium species were detected for the 0.4CrZr, but only one polymeric chromium was observed for 0.8CrZr [III]. The presence of Cr^{5+} species [9,53] might also explain the complexity of the chromate bands on the chromia/zirconia. For the alumina- and zirconia/alumina-supported catalysts, Raman spectroscopy revealed polymeric chromium species of just one type and the bands were less complex than for the zirconia-supported catalysts.

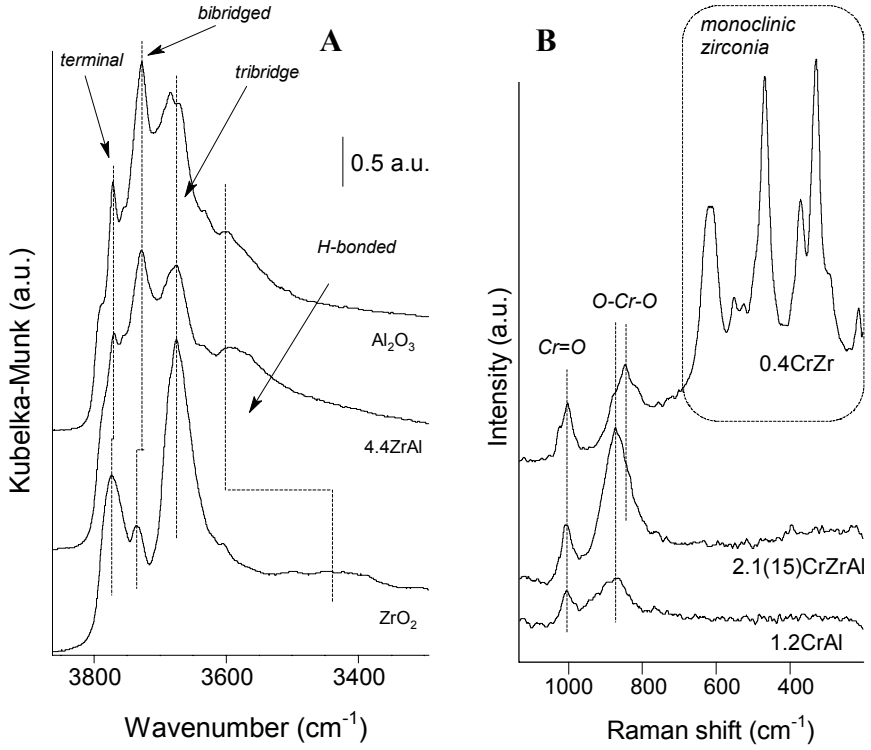

Figure 6. (A) DRIFT spectra for the calcined supports in the hydroxyl region and (B) Raman spectra for the calcined 0.4CrZr, 2.1(15)CrZrAl, and 1.2CrAl catalysts. The spectrum of the quartz window has been subtracted from the Raman spectra. [III]

5.2 Acid–base properties of the supports and catalysts

5.2.1 Surface of monoclinic zirconia

The surface of monoclinic zirconia was further studied by DFT. As an example, Figure 7 presents the model used for the bare ($\bar{1}11$) surface. Three c.u.s Zr^{4+} sites (1, 3, and 4) and three c.u.s. O^{2-} sites (A, C, and D) were present in the unit cell. On the bare ($\bar{1}01$) surface, in turn, there were two different types of c.u.s Zr^{4+} sites and three different c.u.s. O^{2-} sites per unit cell. All c.u.s. Zr^{4+} sites on the ($\bar{1}11$) surface were six-fold coordinated, whereas those on the ($\bar{1}01$) surface were five- and six-fold coordinated. The c.u.s Zr^{4+} sites are Lewis acid sites, while the c.u.s. O^{2-} sites are Lewis base sites. The adsorption of water was studied for both surfaces.

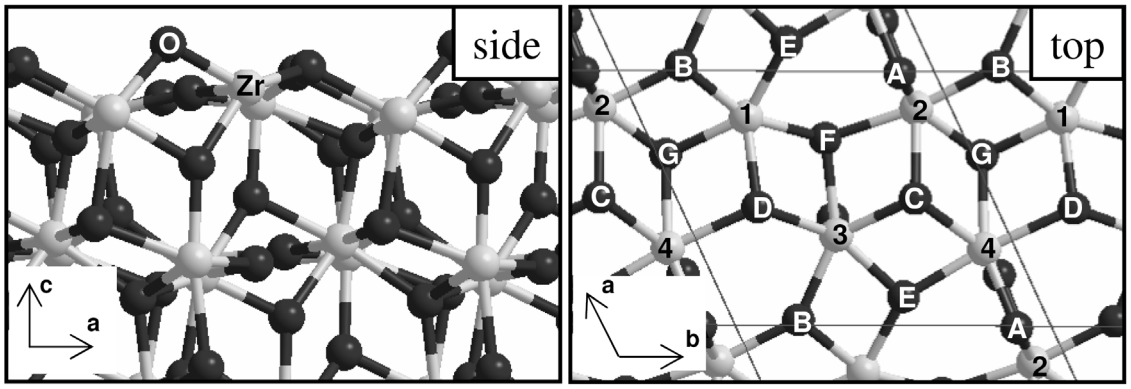

Figure 7. Relaxed model for the ($\bar{1}11$) surface (side and top views). The zirconium and oxygen atoms are presented in light and dark gray, respectively. The underlying atoms have been removed from the top view for clarity. The unit cell is presented in the top view with gray lines. [I]

Figure 8 presents the adsorption energy of water per water molecule as a function of coverage on the ($\bar{1}11$) and ($\bar{1}01$) surfaces. As well, it shows the side views of the hydrated ($\bar{1}11$) surfaces containing 1–4 water molecules per unit cell, i.e., θ = 0.25–1, and a top view of the model surface containing one dissociatively adsorbed water molecule.

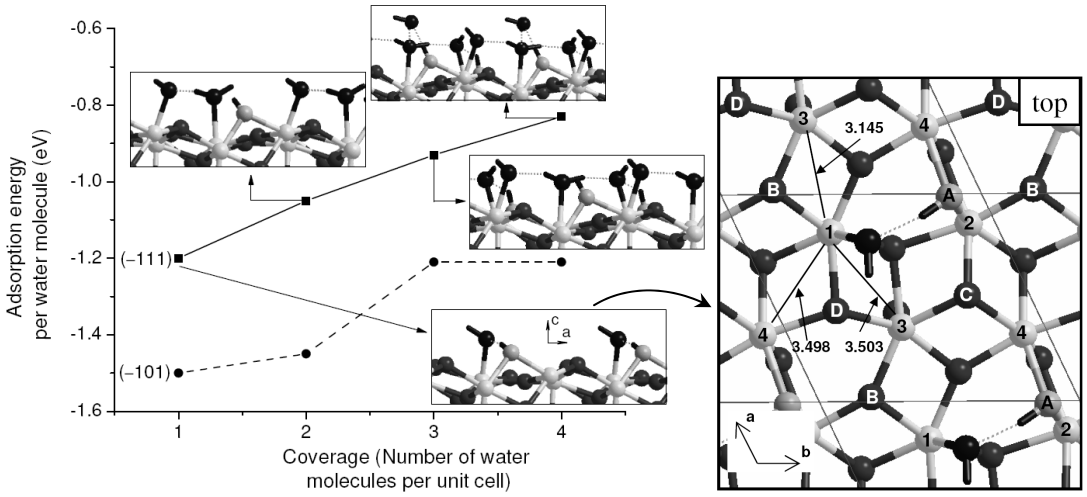

Figure 8. Adsorption energy (eV) per water molecule as a function of coverage on the ($\bar{1}11$) and ($\bar{1}01$) surfaces of zirconia, and the side views of the hydrated ($\bar{1}11$) surfaces (left). Top view of the hydrated ($\bar{1}11$) surface containing one dissociatively adsorbed water molecule (right). [I,II]

For both surfaces the adsorption energy per water molecule decreased with increasing coverage, in agreement with similar studies on other metal oxides [22–27]. The adsorption energies were lower for the ($\bar{1}11$) than the ($\bar{1}01$) surface in accordance with its higher stability, i.e., lower reactivity of the ($\bar{1}11$) surface. For both surfaces the adsorption of one molecule of water was dissociative, with the formation of terminal and bibridged hydroxyls. With increasing water coverage the molecular adsorption of water became more favorable, and for the ($\bar{1}11$) surface the formation of a second layer of adsorbed water was observed at $\theta = 1$. The higher reactivity of the ($\bar{1}01$) surface resulted in a preference for dissociative adsorption at higher coverage than for the ($\bar{1}11$) surface. The surfaces obtained by DFT were in good agreement with previous results for monoclinic zirconia [67,68] and monoclinic hafnia [25]. In addition, the theoretical results were in good agreement with the experimental ones obtained by in situ DRIFTS: the hydroxyls were calculated to vibrate between 3822 and 3743 cm^{-1} (terminal), between 3755 and 3568 cm^{-1} (bibridged), and between 3647 and 3498 cm^{-1} (tribridged), and the experimental bands were observed at 3774, 3738, and 3675 cm^{-1} (for the terminal, bibridged, and tribridged hydroxyls, respectively) (see Figure 6A). In agreement with the experimental results, the calculations also indicated that hydrogen

bonding pairs would shift the vibrational frequencies toward lower wavenumbers by 100–500 cm^{-1}.

The thermodynamic analysis indicated that at atmospheric pressure the temperature of desorption of water from the $(\bar{1}11)$ and $(\bar{1}01)$ surfaces was ~360 and ~480 °C, respectively. However, hydroxyls have been found to exist on the zirconia surface even after evacuation at 500 °C [69]. And according to the in situ DRIFTS results, the hydroxyls are stable under atmospheric pressure even at ~600 °C [I]. This disagreement is likely to originate from the presence of other exposed planes and defects in the real catalyst, responsible for more stable hydroxyl groups. Qualitatively, however, the computed surfaces were in good agreement with the experimental results. The $(\bar{1}11)$ surface containing one dissociatively adsorbed water molecule per unit cell (see Figure 8) was used in the studies on carbon dioxide and carbon monoxide adsorption. This surface was chosen because (i) it contained different types of surface sites: two hydroxyl groups (Brønsted acidic or basic), two c.u.s Zr^{4+} (Lewis acid site), and two c.u.s. O^{2-} (Lewis base site), and (ii) the thermodynamic analysis indicated that a low coverage surface would be stable at high temperatures.

5.2.2 Basic surface sites of zirconia, alumina, and zirconia/alumina

In situ DRIFTS measurements of carbon dioxide adsorption were done to study the basic sites for the zirconia [II], alumina [unpublished results], and 4.4ZrAl [unpublished results] supports. The basic surface sites of zirconia were further studied by DFT [II]. The infrared bands and the reactive basic sites were identified according to the results of Bachiller-Baeza et al. [49]. Figure 9 presents in situ DRIFT spectra recorded at 30 °C for the alumina, 4.4ZrAl, and zirconia supports after the adsorption of carbon dioxide. The spectra were recorded after 30 min of flushing with nitrogen.

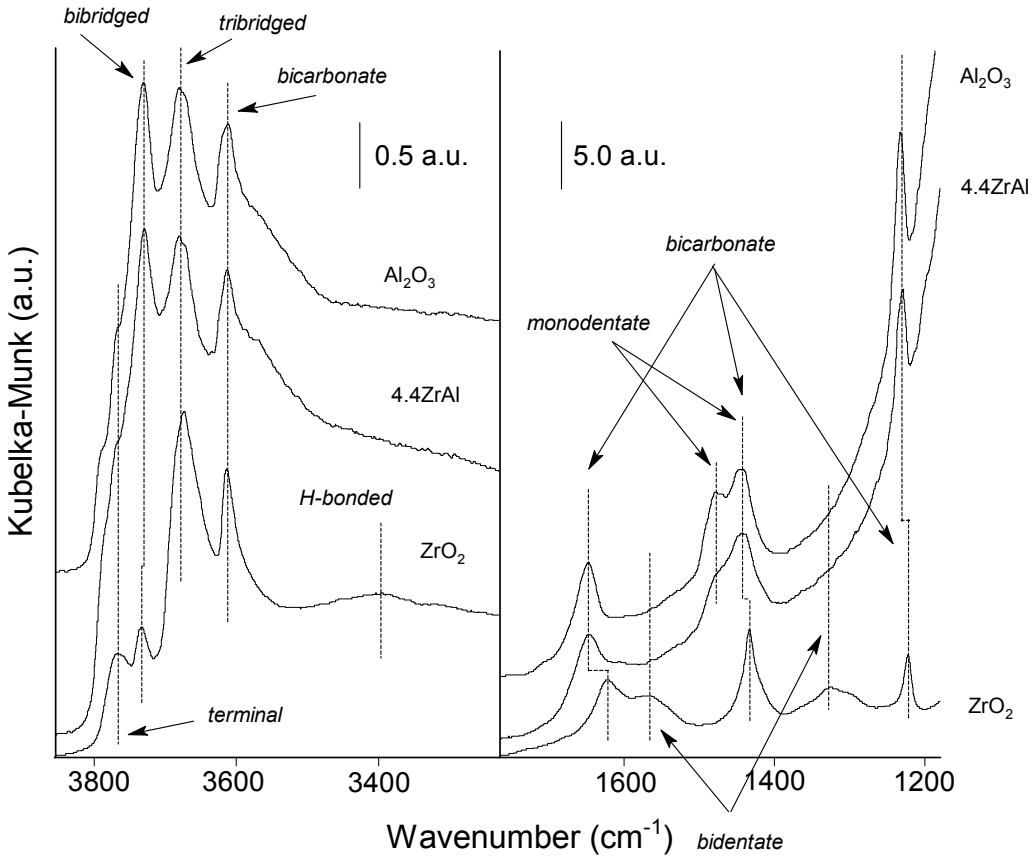

Figure 9. Measurement of carbon dioxide adsorption by in situ DRIFTS on the alumina, 4.4ZrAl, and zirconia supports. The spectra were recorded after a 30 min nitrogen flush at 30 °C.

All supports showed the formation of bicarbonate species. For the alumina-containing supports these species were observed from the bands at 3613 (ν(OH)), 1647 (ν_{as}(CO)), 1450(ν_s(CO)), and 1232 cm^{-1} (δ(OH)), and for the zirconia support from the bands of at 3611, 1619, 1436, and 1223 cm^{-1}. The bicarbonates were formed in a reaction between the terminal, basic hydroxyl groups and carbon dioxide. The decrease in the intensity of the bands of the terminal hydroxyl groups upon reaction (see Figure 6A, p. 40, for comparison) was in agreement with the assignment. For the alumina and 4.4ZrAl supports an additional band was observed at 1477 cm^{-1}. This band was assigned to a ν_{as}(CO) vibration of monodentate carbonates formed on the highly basic c.u.s. O^{2-} species. For the alumina-containing supports the band at 1450 cm^{-1} was considered to originate from both the bicarbonate species and the monodentate carbonates. The bands of the monodentate species were better resolved for the alumina support than for the 4.4ZrAl support, possibly indicating that the c.u.s. O^{2-} species were either stronger in

basicity or more numerous for the alumina. The presence of c.u.s. O^{2-} species was not observed for the zirconia support. However, bidentate carbonate species were observed from bands at 1559 (ν_{as}(CO)) and 1322 cm^{-1} (ν_{s}(CO)). These species were formed in a reaction between an acid–base pair (c.u.s. Zr^{4+}–O^{2-}) and the carbon dioxide. Hence, the basic surface sites of the 4.4ZrAl support more strongly resemble those of alumina than those of zirconia. The bicarbonate species were stable only up to ~175 °C, whereas the mono- and bidentate carbonate species were stable up to ~250 and ~400 °C, respectively (not shown). The order of stability of the different species supports the assignment of the bands at 1477 and 1450 cm^{-1} observed for the alumina-containing supports to monodentate rather than polydentate carbonates, for polydentate carbonates should be thermally more stable [49].

The interaction of carbon dioxide with the monoclinic zirconia surface containing one dissociatively adsorbed water molecule (see Figure 8) was studied by DFT to further elucidate the properties of the zirconia surface, as well as to clarify the structure of the carbonaceous species [II]. Figure 10 presents the structures obtained for the (bi)carbonate species. The theoretical results were validated by comparing the calculated and experimentally observed vibrational frequencies (see Table 4).

The theoretical results were in good agreement with the experimental results. The bicarbonate species were indeed formed in a reaction between the terminal, basic hydroxyl groups and gaseous acidic carbon dioxide. However, according to the theoretical results (both energetics and vibrational frequencies), the bicarbonates were bidentate and bound to two c.u.s. Zr^{4+} (structure I). This is in contrast to the monodentate coordination suggested previously [49]. According to the calculations, the monodentate bicarbonates (structure V) were highly unstable. Again according to the calculations, the most stable carbonate species were polydentate (structure II). However, the difference in adsorption energies between the polydentate and bidentate carbonates (structure III) was small. In addition, the experimental DRIFT bands assigned to the bidentate carbonates were broad, making it difficult to distinguish between the two structures. It is suggested, however, that the formation of polydentate carbonates requires the presence of an extended acid–base pair (Zr^{4+}–O^{2-}–Zr^{4+}) instead of the previously suggested [49] closely spaced c.u.s. Zr^{4+} sites. Nevertheless, the formation of

both structures requires a Lewis acid–base pair: Zr^{4+}–O^{2-}–Zr^{4+} for the polydentate and Zr^{4+}–O^{2-} for bidentate carbonates. In agreement with the experimental results, no monodenate carbonate species were formed on monoclinic zirconia confirming the absence of highly basic c.u.s. O^{2-} sites on zirconia.

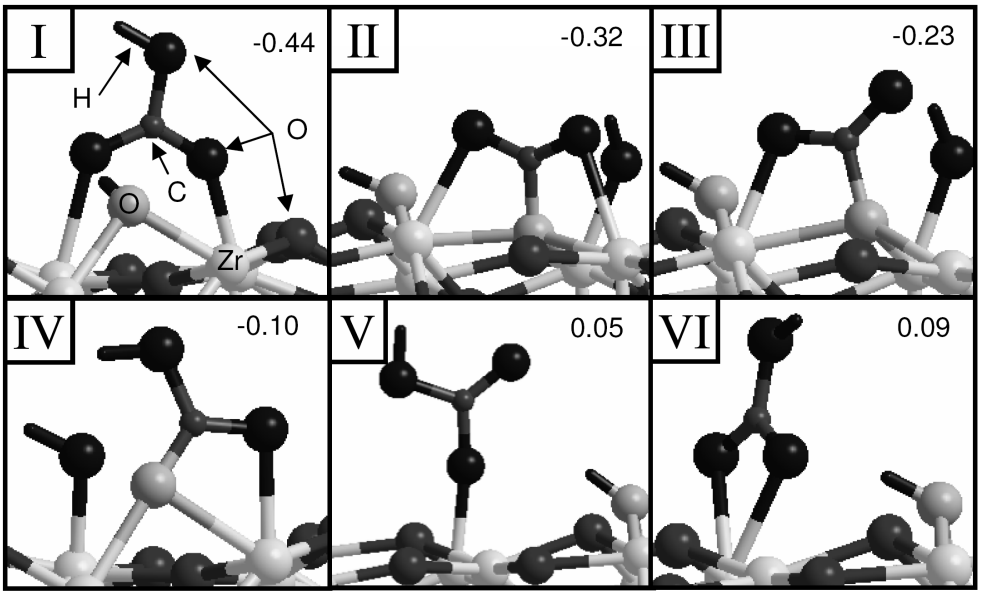

Figure 10. Most stable (bi)carbonate structures in order of stability for the monoclinic ($\bar{1}11$) surface of zirconia. The adsorption energies are presented in eV. (I) Bidentate bicarbonate bound to two zirconium atoms, (II) polydentate carbonate, (III) bidentate carbonate, (IV) bidentate bicarbonate bound to zirconium and lattice oxygen, (V) monodentate bicarbonate, and (VI) bidentate bicarbonate bound to one zirconium atom. [II]

Table 4. Comparison of experimentally observed and calculated infrared frequencies (cm^{-1}) for (bi)carbonate species. The numbers refer to the structures in Figure 10. [II]

	experimental		calculated					
	bicarbonate	bidentate carbonate	I	II	III	IV	V	VI
ν(OH)	3611	---	3686	---	---	3750	3708	3764
ν_{as}(CO)	1619	1559	1600	1667	1791	1579	1728	1619
ν_{s}(CO)	1436	1322	1386	1239	1158	1428	1307	1412
δ(OH)	1223	---	1204	---	---	1194	1126	1197
$\Delta\nu=\nu_{as}-\nu_{s}$	183	237	213	428	633	151	421	207

5.2.3 Acidic surface sites of zirconia, alumina, and zirconia/alumina

The adsorption of carbon monoxide and the formation of formates were studied on monoclinic zirconia [II], alumina [unpublished results], and 4.4ZrAl [unpublished results] by in situ DRIFTS to study the acidic surface sites. The spectra are not shown for the sake of brevity. The experimental bands were identified according to previous reports [70–72].

The temperature for the formation of formates depended on the support material. The bands assigned to formates were first observed at ~175 °C for zirconia, at ~225 °C for alumina, and at ~300 °C for 4.4ZrAl suggesting that zirconia had the most acidic hydroxyl groups. The formate bands reached their maximum intensities around 400 °C and were observed up to ~500 °C. The formation of low intensity bands assigned to bicarbonates was also observed. The formation of these bands was accompanied by the formation of gaseous carbon dioxide observed by MS (not shown). The formation of bicarbonates was, therefore, assigned to the adsorption of the detected carbon dioxide. The temperature for the bicarbonate formation was ~150 °C for 4.4ZrAl, ~175 °C for alumina, and ~225 °C for zirconia, and the bands were observed up to ~250 °C on all supports. The formation of carbon dioxide was assigned to basic surface sites, which were stronger on alumina-containing supports than on zirconia.

DFT calculations were performed to further study the acidic sites of monoclinic zirconia, as well as to clarify the structure of the formates [II]. Figure 11 presents the most stable formate structures and Table 5 compares the calculated vibrational frequencies with the experimental ones. Note that the calculations are not able to produce the combination modes (ν_{as}(COO)+ν_s(COO) and ν_s(COO)+δ(CH)); these were calculated by summing the corresponding frequencies.

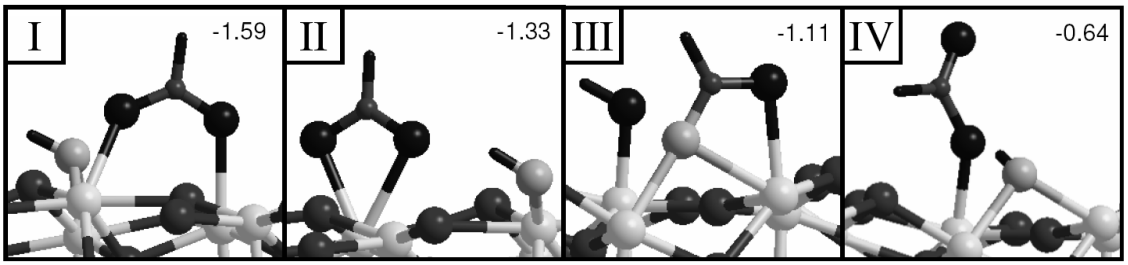

Figure 11. The most stable formate structures in order of stability for the monoclinic ($\bar{1}11$) surface of zirconia. The adsorption energies are presented in eV. (I) Bidentate formate bound to two surface zirconium atoms, (II) bidentate formate bound to one zirconium atom, (III) bidentate formate bound to zirconium and lattice oxygen, and (IV) monodentate formate. The atoms are color-coded as in Figure 10. [II].

Table 5. Comparison of experimentally observed and calculated infrared frequencies (cm^{-1}) for formate species. The numbers refer to the structures in Figure 11. [II]

	exp.	I	II	III	IV
$\nu_{as}(COO)+\nu_s(COO)$ [a]	2964	2915	2845	2765	2843
$\nu(CH)$	2881	2974	2997	3138	2892
$\nu_s(COO)+\delta(CH)$ [a]	2747	2754	2676	2504	2473
$\nu_{as}(COO)$	1564	1555	1544	1585	1717
$\delta(CH)$	1384	1394	1375	1324	1347
$\nu_s(COO)$	1365	1360	1301	1180	1126
out of plane	n.o. [b]	1010	995	958	983
$\Delta\nu=\nu_{as}-\nu_s$	199	195	243	406	591

[a] Combination modes are not available in the calculations, and the values were obtained by summing the corresponding frequencies.

[b] n.o. = not observed

As for the bicarbonates, the most stable calculated structure for formates was bidentate, bound to two c.u.s Zr^{4+} (structure I), and formed in a reaction with the terminal hydroxyl groups. The calculated vibrational frequencies for this structure were in excellent agreement with the experimental bands. In an earlier study [73] it has been suggested that, on cubic zirconia (yttrium-stabilized), the neighboring Zr^{4+} sites are too far apart for such structures to be stable and that the formate species must be bidentate

but bound to one surface c.u.s. Zr^{4+} as in structure II. However, the distances between the neighboring Zr^{4+} sites were shorter (3.503 Å for the longest distance) on the monoclinic ($\bar{1}11$) surface (see Figure 8) than on the cubic zirconia (3.64 Å [73]). The preference to bridge between two c.u.s. sites has previously been reported for ZnO [74] and TiO_2 [75] on the basis of theoretical results. Here, however, the differences in adsorption energies for the two bidentate structures were small, and the calculated vibrational frequencies for structure II were not significantly different from the experimental values. Probably, therefore, at high formate loadings, where there would be a lack of available neighboring c.u.s. Zr^{4+}, structure II would be present as well [II]. Neither structure III nor structure IV was considered [II] stable enough to exist on the surface long enough to be detected in the experiments. The carbon dioxide and carbon monoxide adsorption results indicate that the hydroxyl groups of monoclinic zirconia are amphoteric in character. This is in agreement with previous results [50].

5.2.4 Acid–base sites and surface composition of the supports and catalysts

All supports and chromia catalysts, except 2.7CrZr, were studied in methanol adsorption–desorption and in temperature-dependent methanol adsorption experiments [III]. Figure 12 presents the methoxy species observed by in situ DRIFTS for the supports (A) at 200 °C and for the chromia catalysts containing 1–2 at_{Cr}/nm^2 (B) at 100 °C under nitrogen during the adsorption–desorption experiments. The spectra for the supports are presented at 200 °C because of the presence of chemisorbed methanol on the alumina-containing supports at lower temperatures. The bands of chemisorbed methanol were less intense for the chromia catalysts.

At 200 °C, bands originating from zirconium- and aluminum-bound methoxies were observed for the zirconia and alumina supports and both types of methoxies were observed for the 4.4ZrAl support (Figure 12A). Zirconia was the only support to show additional activity toward methanol at low temperature, and the formation of formate species was observed. Formates were not observed below ~250 °C on the alumina-containing supports.

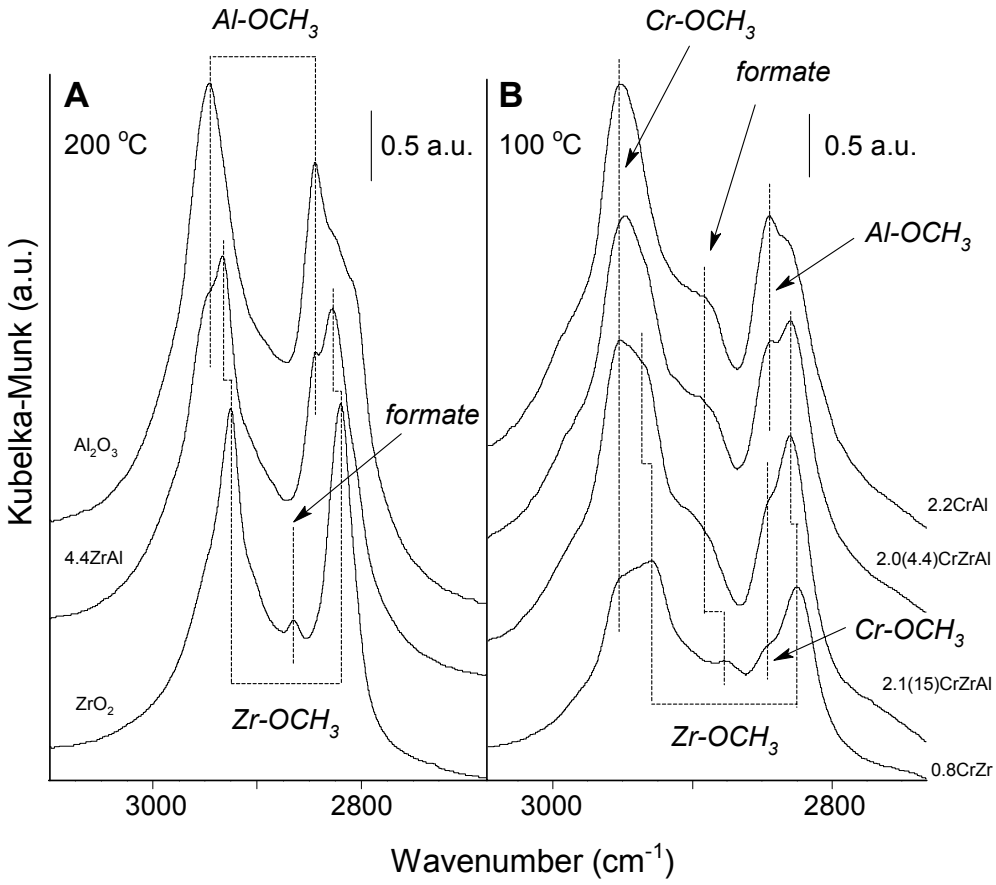

Figure 12. Methoxy species for the supports (A) at 200 °C and the chromia catalysts (B) at 100 °C observed by in situ DRIFTS. Spectra recorded under nitrogen during measurements of adsorption–desorption. [III]

The formation of formate species on the zirconia support at 100 °C may indicate more active sites (in strength or number) on the zirconia surface than on the alumina or 4.4ZrAl surfaces. As for the alumina-containing supports, the formation of formates on Ga_2O_3 [76] under methanol required a temperature of 200 °C. For zirconia supported on silica [77], in turn, the formation of formates required prolonged times under methanol at 250 °C. The decomposition of methoxy species on these oxides was considered to involve lattice oxygen species capable of abstracting hydrogen and forming methylenebisoxy (H_2COO) species that were further dehydrogenated to formates [76,77]. A similar reaction is proposed to occur on the alumina-containing supports, and the detection of monodentate carbonates, i.e., of highly basic c.u.s. O^{2-}, for these supports is in agreement with the suggested reaction mechanism. Highly basic c.u.s. O^{2-}

species were not observed for zirconia, either in the carbon dioxide adsorption experiments or in the DFT study [II]. However, if on zirconia the methoxies were bound to the Lewis acid part of the acid–base pair (c.u.s. Zr^{4+}–O^{2-} or c.u.s. Zr^{4+}–O^{2-}–Zr^{4+}) observed in the carbon dioxide adsorption measurements, the Lewis base part could provide the active site for the abstraction of hydrogen from the methoxy. The low temperature for the formate formation might be explained by the short distance between c.u.s. Zr^{4+} and c.u.s. O^{2-} in the acid–base pair. No acid–base pairs were observed for the alumina-containing supports, and one might assume that there the c.u.s. sites are further apart and the higher temperatures are required at least partially for this reason. The DFT study also indicated [II] that the hydroxyl groups of zirconia are highly reactive and these surface species might also be responsible for the higher activity of zirconia.

Chromium-bound methoxy species were observed for the chromia catalysts (Figure 12B) but only at 100 °C. At higher temperatures the chromium-bound methoxy species reacted further, most likely to formates. However, all chromia catalysts showed some formate species already at 100 °C suggesting that more active sites were created by chromia deposition. Bands originating from zirconium- and aluminum-bound methoxies were observed for the zirconia- and alumina-supported catalysts, respectively, and both zirconium- and aluminum-bound methoxies were observed for the 2.0(4.4)CrZrAl. The Al-bound methoxies were not observed for the 2.1(15)CrZrAl suggesting either that the alumina surface was fully covered by the deposited zirconia and chromia or that the aluminum species were unable to react with methanol.

In the temperature-dependent measurements of methanol adsorption, in situ DRIFTS was used to study the formation of surface species and MS the formation of gaseous reaction products. In addition in situ Raman–MS measurements were used to study the desorption of the surface species and the formation of reaction products. According to Wang and Wachs [64], the formation of carbon dioxide, formaldehyde (HCOH), and dimethyl ether (DME) is indicative of the presence of basic, redox, and Lewis acid surface sites, respectively. The formation of HCOH observed in the in situ Raman–MS measurements was assigned to the redox properties of chromium. Table 6 presents the temperature ranges for the formation of DME, carbon dioxide, and hydrogen in the temperature-dependent adsorption experiments.

Table 6. Temperature ranges (°C) for the formation of DME, CO_2, and H_2 in the temperature-dependent measurements of methanol adsorption. The formation of DME and CO_2 is indicative of Lewis acid and base sites, respectively. [III]

sample	DME (Lewis acid sites)	CO_2 (basic sites)	H_2
Al_2O_3	150-300	450-500	450-580 (300-580) [a]
4.4ZrAl	175-300	150-580	(300-580) [a]
ZrO_2	---	---	450-580 (250-580) [a]
1.2CrAl	200-300	300-400 (250-580) [a]	325-580
2.1(15)CrZrAl	250-300	300-400 (250-580) [a]	325-580
0.8CrZr	---	(300-580) [a]	325-580

[a] The temperatures in brackets indicate the whole temperature range of formation and the values in front of them the temperature range where the formation was strongest.

The alumina support had the strongest Lewis acid surface sites (i.e., the lowest temperature of formation for DME) and the deposition of both zirconia and chromia reduced the Lewis acidity (number or strength of the species), seen as increase in the temperature of formation for DME. These results are in accordance with those of Damyanova et al. [10], who found that zirconia deposition on alumina decreases the concentration of the strong Lewis acid sites. No DME was detected for the zirconia support or the 0.8CrZr catalyst. The formation of carbon dioxide was observed for all catalysts and supports except the zirconia. The absence of any reaction products formed on Lewis acid or base surface sites of the zirconia support suggests that the methanol adsorption–desorption measurements were unable to probe the acid–base pairs (c.u.s. Zr^{4+}–O^{2-}) that were detected on zirconia by the carbon dioxide adsorption measurements [II]. In addition, since all supports showed the presence of basic terminal hydroxyl groups in the carbon dioxide adsorption measurements, but only the alumina and 4.4ZrAl supports exhibited basic properties in the methanol adsorption–desorption measurements, the basic sites forming carbon dioxide in these measurements on the alumina-containing supports must have been mainly the c.u.s. O^{2-} species. However, 4.4ZrAl produced carbon dioxide over a wider temperature range than the alumina in the methanol adsorption–desorption measurements suggesting its higher basicity. Lower basicity was suggested on the basis of the carbon dioxide adsorption measurements. On the basis of the temperature for the formation of carbon dioxide in the carbon monoxide adsorption measurements, the 4.4ZrAl was again more basic that the alumina. Hence,

the carbon dioxide adsorption only reveals the strongest Lewis base sites, whereas the temperature-dependent methanol adsorption probes the basic sites of varying strength. The total basicity of zirconia/alumina is, therefore, higher than the total basicity of alumina, although some very strong Lewis base sites exist on the alumina surface.

The formation of carbon dioxide on the chromia catalysts was partially due to the reduction of the chromates (at ~325 °C according to the isobutane measurements [IV,V,4]), but the chromium species may also have increased the basicity of the catalysts. The increased basicity may explain the increased activity for the formation of formates that was observed in the methanol adsorption–desorption measurements for the chromia catalysts. Hydrogen was suggested to form on the Cr^{3+} species and during the decomposition of formates [III,78]. The XPS measurements [III] ruled out the formation of a mixed oxide, but the infrared measurements showed similarities between the zirconia/alumina- and alumina-supported catalysts. It was concluded [III] that there is a strong interaction between the alumina and zirconia of the zirconia/alumina support and that the acid–base properties of zirconia/alumina resemble those of alumina rather than those of zirconia.

5.3 Performance in isobutane dehydrogenation

The activity in isobutane dehydrogenation was studied for all supports and for the chromia catalysts containing 1–2 at_{Cr}/nm^2 [V]. In situ DRIFTS measurements with isobutane were performed for all supports and all chromia catalysts [IV,V], and in situ Raman–MS measurements were performed for the 0.8CrZr, 2.1(15)CrZrAl, and 1.2CrAl catalysts [V].

5.3.1 Activities in dehydrogenation

Figure 13 presents a summary of the performance of the supports and catalysts during dehydrogenation of isobutane. The supports were slightly active in the dehydrogenation reaction, with zirconia the most active support. The alumina and 4.4ZrAl supports exhibited lower, comparable activities. The order of reactivity under isobutane was in agreement with that under methanol for the formation of formates [IV]. The acid–base

pairs (c.u.s. Zr^{4+}–O^{2-}) or the amphoteric hydroxyls observed on the zirconia, could also be the active sites for the dehydrogenation reaction. The alumina-containing supports, but not zirconia, were also active in the cracking reaction. The cracking activity might originate from similar acidic hydroxyl species, as observed by DRIFTS (see Figure 6A, p. 40), on the alumina-containing supports. The coke content after dehydrogenation was highest on alumina and lowest on zirconia. The amount of coke on the supports followed the Lewis acidity of the material, as determined by the methanol adsorption–desorption measurements [III], not the dehydrogenation activity. It was concluded [V] that the deposition of zirconia was beneficial for the dehydrogenation performance of the alumina-containing supports by reducing the Lewis acidity that was responsible for coke deposition.

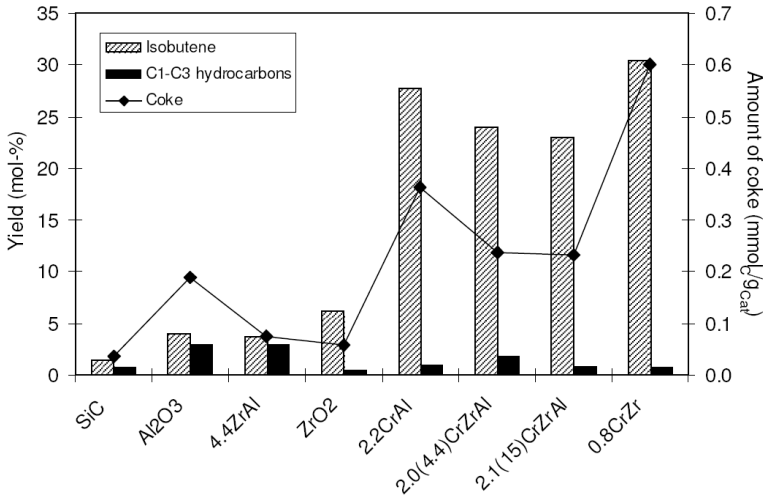

Figure 13. Summary of the performance of supports and chromia catalysts during dehydrogenation. The striped columns present the yield of isobutene and the black columns the yield of C_1–C_3-hydrocarbons (cracking products) (left axis). The isobutene yield was measured at 2 min on stream, and the C_1–C_3 yield is an average of observed amounts between 2 and 3 min on stream. ♦ presents the amount of coke (as carbon) formed during the dehydrogenation (right axis). The connecting line has been added to guide the eye. [V]

All chromia catalysts were active in the dehydrogenation reaction. The 0.8CrZr catalyst was the most active, even though it had the lowest chromium content in weight percentage. The activity might originate from the more easily available chromium species or from a beneficial interaction between the zirconia support and the chromium species. In the case of the oxidative dehydrogenation (ODH) of *n*-butane it was noted

[54] that the activity of vanadia catalysts (TiO_2>ZrO_2>Al_2O_3>SiO_2) increases with the decreasing electronegativity of the support, because the more basic the V–O–support bonds the more efficient they are in activating the C–H bonds of the hydrocarbon. Although these ODH results do not allow a conclusion on the effect of support on dehydrogenation, owing to the different reaction conditions, it is reasonable to think that the different electronegativities of the present support materials would influence the dehydrogenation reaction in the same direction.

The deposition of zirconia was not beneficial for the activity of the chromia catalysts: the zirconia/alumina-supported catalysts were less active that the 2.2CrAl catalyst. This is in contrast to the results of Gaspar and Dieguez [42], who reported a slight increase in the dehydrogenation activity when zirconia/alumina containing 1.6 at_{Zr}/nm^2 and no zirconia crystallites (XRD) was used as the support in place of alumina. However, they reported the activities in turnover numbers (TON) without giving detailed information on the reaction conditions. Furthermore, the number of active sites on the catalyst surface required to calculate the TON values, were determined by oxygen chemisorption. In addition, no explanation was presented for the beneficial effect, and the characterization results they report do not allow speculation here. In agreement with our findings, Burch and Loader [43] observed zirconia deposition on alumina to decrease the activity of rhodium catalysts supported on alumina and zirconia in the reduction of nitrogen oxide and in the combustion of methane, respectively. The decrease in the activity was assigned to the incomplete monolayer of zirconia that modified the active surface species. The presence of zirconia interfered with the interaction between alumina and rhodium important for high activity in the reduction of nitrogen oxide to nitrogen. On the other hand, the interference was not high enough to prevent the interaction between alumina and rhodium completely, and this caused the low activity in the combustion of methane. Although such conclusions are not as easily drawn for chromia catalysts, it appears that, even for the zirconia/alumina-supported catalyst with highest zirconia surface density (5.2 at_{Zr}/nm^2) the chromium species are in interaction with both the zirconia and the alumina, with the result that the activity in dehydrogenation is lower than that of the zirconia- or alumina-supported catalysts.

The yields of the cracking products with the chromia catalysts were of the same order of magnitude as with the inert silicon carbide, and the formation was, therefore, assigned to thermal reactions [V]. The amount of coke that formed followed the dehydrogenation activity of the catalysts, in contrast to the findings for the supports, where the amount of coke was dependent on the Lewis acidity. It was concluded [V] that, for the chromia catalysts, the coke was formed from adsorbed isobutene. The hydrogen content of the coke on the catalysts was lowest for the 0.8CrZr catalyst.

5.3.2 Formation of carbonaceous surface species in dehydrogenation

The in situ DRIFTS measurements of isobutane were performed as (i) temperature-dependent or (ii) time-dependent studies [IV,V]. The in situ Raman–MS measurements were done at constant temperature of 570 °C. In the temperature-dependent experiments, oxygenated carbonaceous surface species were formed on all catalysts and supports. Figure 14 presents a reaction scheme for the formation of these species in accordance with the results of Ermini et al. [79] for alumina, Finocchio et al. [71,72] for $MgCr_2O_4$, and Airaksinen [4] for chromia/alumina catalysts during isobutane and propane dehydrogenation.

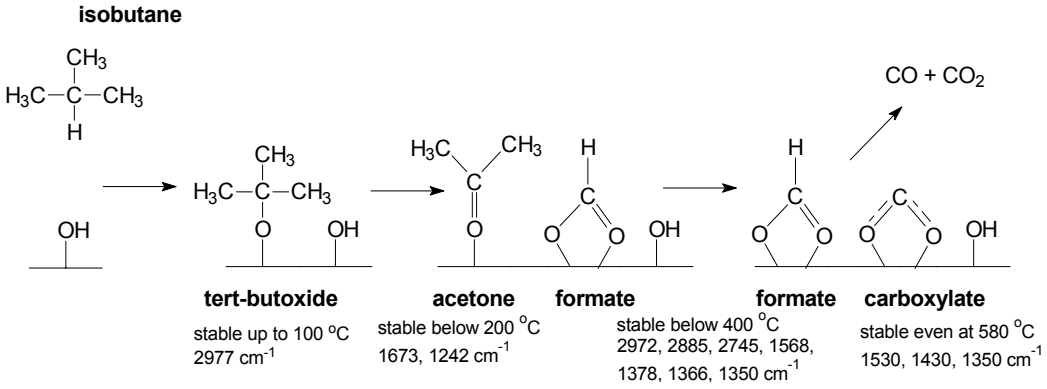

Figure 14. Reaction mechanism suggested for the formation of oxygenated carbonaceous species. The mechanism is based on the results of Ermini et al. [79], Finocchio et al. [71,72], and Airaksinen [4]. The DRIFTS bands observed for 0.8CrZr are presented for each species. [IV,V]

The bands of the carboxylate-type species presented in Figure 14 have earlier been assigned to acetates [IV,4,71,72,79]. The carboxylates are not formed during adsorption of carbon dioxide or carbon monoxide on the catalysts [II], but their formation seems to

require the presence of hydrocarbons. It was concluded [IV,V,4] that the oxygenated species, formed during the reduction of the chromates and to lesser extent on the hydroxyl species and possibly on the acid–base pairs on the supports, were spectators and not dehydrogenation products or reaction intermediates.

The chromia species were reduced [IV,V,4] at ~325 °C, where their bands disappeared from the spectra. At 400 °C the bands of adsorbed isobutene were observed for the chromia/zirconia catalysts, and dehydrogenation products were detected by MS [IV,V]. These bands were also observed for the chromia/zirconia/alumina but at a slightly higher temperature [V]. They were not observed for chromia/alumina [V]. At higher temperatures all catalysts showed the formation of aliphatic (bands at ~2930 and 2980 cm^{-1}) and aromatic/unsaturated (~3060 cm^{-1}) hydrocarbon species assignable to coke [IV,V].

Figure 15 presents a comparison of bands observed in the C–H stretching region during the time-dependent measurements for the calcined chromia catalysts containing 1–2 at_{Cr}/nm^2 [IV,V]. Aliphatic (~2930 and 2980 cm^{-1}) and carboxylate-type (~1530, 1430, and 1350 cm^{-1}, not shown) surface species were formed after a short time on isobutane stream, whereas the formation of the unsaturated/aromatic (~3060 cm^{-1}) species required a longer time. In agreement with the dehydrogenation activity measurements, the coke content was the highest for the 0.8CrZr catalyst. The alumina-containing catalysts showed an additional band (~3100 cm^{-1}), possibly originating from adsorbed isobutene. The alumina-containing catalysts also showed bands for both methyl- ($–CH_3$, ~2980cm^{-1}) and methylene-type ($>CH_2$, ~2930 cm^{-1}) species [56,80], whereas the 0.8CrZr catalyst showed only methylene-type species ($>CH_2$, 2927 cm^{-1}). The band of the methyl-type species decreased in intensity with increasing time on stream, and it was suggested [V] that it correlated with the amount of hydrogen in the coke, in agreement with the dehydrogenation activity measurements, where the lowest hydrogen content after dehydrogenation was detected for the coke on the 0.8CrZr catalyst.

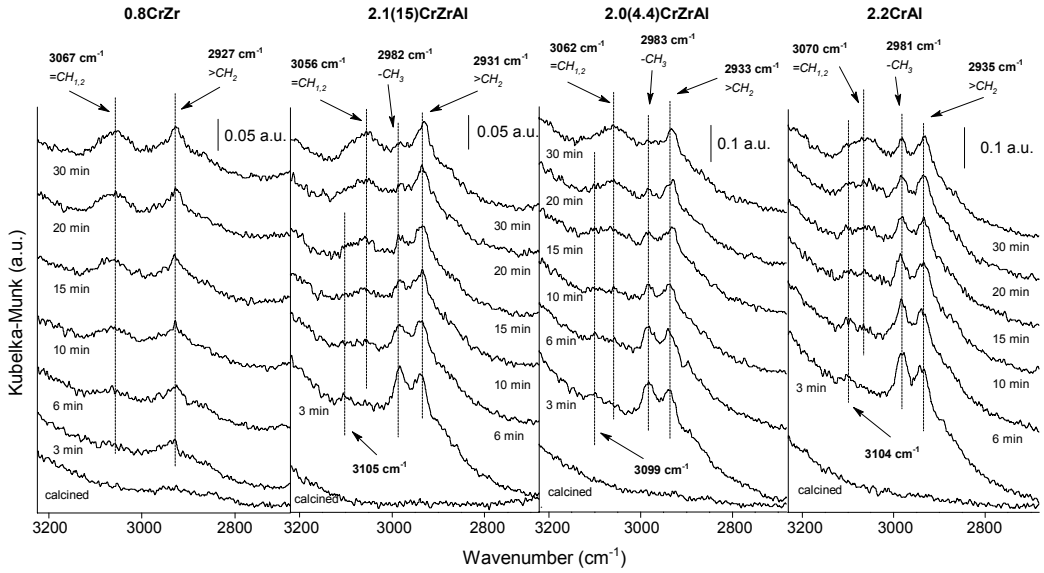

Figure 15. Comparison between the bands observed by in situ DRIFTS in the C–H stretching region during time-dependent measurements at 580 °C. Spectra recorded during nitrogen flushes. [V]

Figure 16 presents the in situ Raman spectra for the 2.1(15)CrZrAl and 0.8CrZr catalysts during dehydrogenation. No spectra were obtained for the alumina-supported catalyst owing to the intense fluorescence under the dehydrogenation conditions [V]. The chromates were reduced immediately after the isobutane feed was directed to the sample at 570 °C. This was in accordance with the time-dependent isobutane measurements by in situ DRIFTS at 580 °C [IV,V]. Carbonaceous surface species were observed for both zirconia- and zirconia/alumina-supported catalysts at ~1585 and ~1339 cm^{-1}, and were assigned [V,81] to pregraphitic carbonaceous species (coke). For the 0.8CrZr catalyst these bands were formed after just 2 min on isobutane stream, but for the 2.1(15)CrZrAl catalyst a longer time was required. These results are in accordance with the in situ DRIFTS and activity measurements [V], which showed a faster rate of coke deposition on the 0.8CrZr catalyst. Similar bands have been observed during propane dehydrogenation on chromia/alumina catalysts with high chromium loading, but only after 20 min on stream [4]. With increasing time on stream the bands of monoclinic zirconia disappeared from the spectra of the 0.8CrZr catalyst. Similar behavior was observed for zirconia-based catalysts by Kuba and Knözinger [81] and this was assigned to the darkening of the sample due to coke formation.

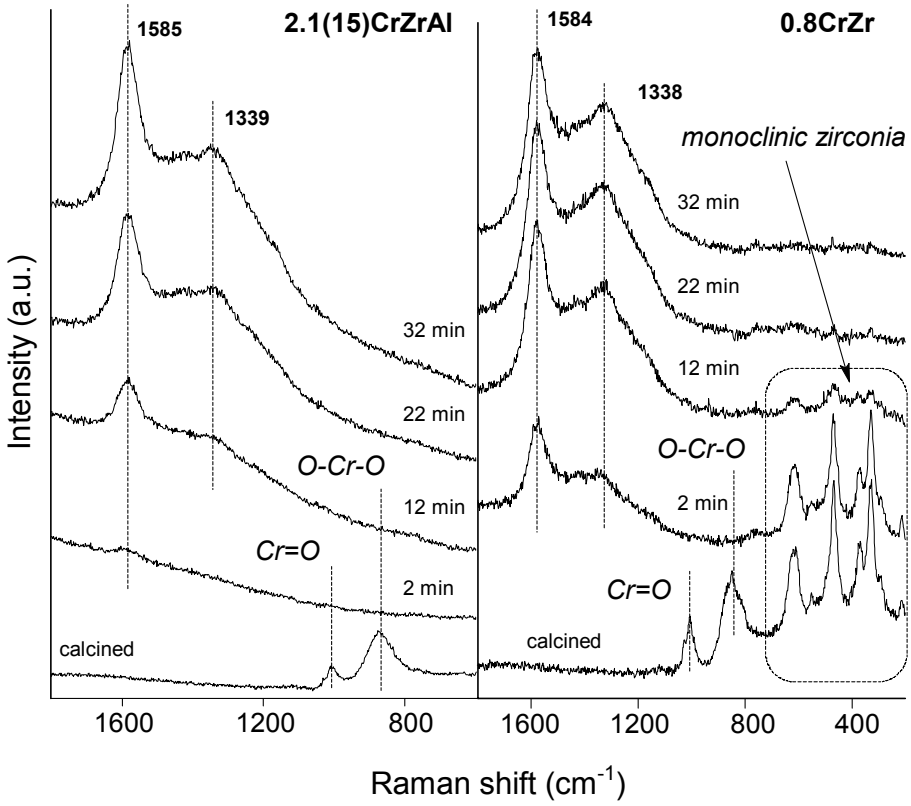

Figure 16. In situ Raman spectra for the 2.1(15)CrZrAl and 0.8CrZr catalysts under dehydrogenation conditions. The spectrum of the quartz window has been subtracted from all spectra. [V]

5.3.3 Effect of hydrogen prereduction in dehydrogenation

Hydrogen prereduction decreased the activity of the catalysts in the dehydrogenation reaction. The alumina-containing catalysts were affected the most. In accordance with the decreased activity, the coke content was also lower on the prereduced than on the calcined catalysts. In the temperature-dependent isobutane measurements by in situ DRIFTS, the formation of the oxygenated carbonaceous surface species was suppressed on the prereduced catalysts, especially on the alumina-containing catalysts, further confirming that the oxygenated carbonaceous surface species were mainly formed during the reduction of the chromates by the hydrocarbon feed. [V]

Figure 17 presents a comparison of in situ DRIFT spectra in the C–H stretching region similar to the comparison in Figure 15, but now for the prereduced catalysts [V]. The

formation of carbonaceous surface species was suppressed on the prereduced alumina-containing catalysts, and this was in accordance with the decreased activity of these catalysts in dehydrogenation. The results suggested [V] that, especially for the alumina-containing supports, hydrogen prereduction was able to inhibit the formation of both the surface species and the dehydrogenation products. The inhibition might originate from the formation of higher concentrations of surface-bound water [4], which competes with isobutane for surface adsorption sites [54].

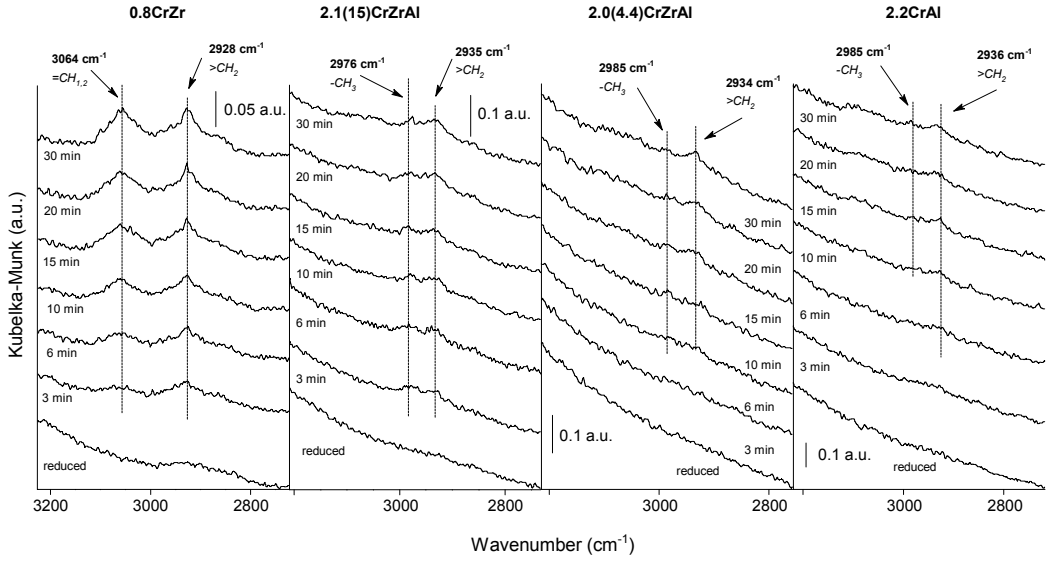

Figure 17. Comparison of bands observed for hydrogen prereduced catalysts by in situ DRIFTS in the C–H stretching region during time-dependent measurements at 580 °C. Spectra recorded during nitrogen flushes. [V]

5.3.4 Effect of acid–base properties in dehydrogenation

Table 7 summarizes the acid–base properties of the supports and their performance in the dehydrogenation of isobutane. Zirconia was the most active and selective support in the dehydrogenation. Zirconia was also the only support that contained pairs of Lewis acid and Lewis base sites. These acid–base pairs, and the amphoteric hydroxyls, were suggested [V] to be the active sites for the dehydrogenation reaction. The amount of coke that was formed during dehydrogenation was lower on zirconia/alumina than on alumina. The deposition of zirconia on alumina, however, did not influence the activity or the selectivity of the alumina support in dehydrogenation. The decrease in the

deposition rate of coke was assigned to the lower Lewis acidity of the 4.4ZrAl than of the alumina, whereas the similar activity and selectivity were assigned to the strong interaction between zirconia and alumina on the zirconia/alumina support resulting in similar acid–base properties [V].

Table 7. Summary of the acid–base properties of the supports and their performance in dehydrogenation [I–V].

	acid–base properties of supports				support performance in dehydrogenation		
support	acidic OH	basic OH	Lewis acid sites	Lewis base sites	activity	selectivity to isobutene	coke
Al_2O_3	+	+	++	+	+	+	+++
4.4ZrAl	+	+	+	++ [a]	+	+	++
ZrO_2	++	+	Lewis acid–base pairs		++	+++	+

[a] **The total basicity (on the basis of experiments with methanol) was higher for 4.4ZrAl than for alumina, although some very strong Lewis base sites exist on alumina surface.**

No direct correlation was found between the acid–base properties of the supports and the performance of the chromia catalysts in dehydrogenation. The deposition of chromia on the supports increased the basicity of all samples, but the used characterization techniques were unable to specifically probe the Cr–O–support bonds. Nonetheless, the support is suggested to influence the performance of the catalyst through these bonds. As was noted [54] for the vanadia catalysts in ODH, the decrease in the electronegativity of the support increased the activity of the catalyst owing to the increased basicity (i.e., capability to activate the C–H bonds) of the V–O–support bonds. This is also suspected to be important for the chromia catalysts in dehydrogenation.

6 SUMMARY

The effect of support material on the performance of chromia dehydrogenation catalysts was investigated with zirconia, alumina, and zirconia/alumina supports. The aim was to elucidate the reasons for the high activity of the chromia/zircona catalysts, and to study the possibility of enhancing the performance of the chromia catalysts by depositing zirconia on alumina. Surface-sensitive characterization methods, modeling, and measurements of dehydrogenation activity were chosen as means to elucidate the effect of support material on the dehydrogenation performance.

The reactive surface sites on monoclinic zirconia were amphoteric hydroxyl groups and acid–base pairs (c.u.s Zr^{4+}–O^{2-}). The acid–base properties were studied by adsorbing carbon dioxide, carbon monoxide, and methanol, and by modeling the interaction of carbon dioxide and carbon monoxide with the surface. Bicarbonates were formed in a reaction between the hydroxyls and acidic carbon dioxide, and formates were formed in a reaction between the hydroxyls and basic carbon monoxide. The most stable bicarbonates and formates were bidentate and bound to two c.u.s Zr^{4+}. Carbon dioxide was also adsorbed on the acid–base pairs, and polydenate and bidentate carbonates were formed.

The reactive surface sites on the alumina and zirconia/alumina supports were hydroxyl groups, Lewis acid sites, and Lewis basic sites. The hydroxyls of alumina and zirconia/alumina exhibited similar basicity to those of zirconia, but their acidity was lower. The Lewis acid and Lewis base sites did not form acid–base pairs on the alumina-containing supports. The Lewis acidity was highest on alumina, whereas the total basicity was highest on zirconia/alumina.

Zirconia support was the most active and selective support material in the dehydrogenation. The acid–base pairs and the amphoteric hydroxyl groups were concluded to influence the activity of zirconia. However, the surface area of zirconia was low. The surface areas of the zirconia/alumina supports were comparable to that of alumina. The lower Lewis acidity of the zirconia/alumina support than that of alumina contributed to the lower rate of coke deposition on zirconia/alumina during the

dehydrogenation reaction. However, the deposition of zirconia on alumina did not decrease the cracking activity or increase the dehydrogenation activity of the alumina support. The lower dehydrogenation activity of the zirconia/alumina support than of the zirconia support may be related to the absence of acid–base pairs, whereas the similar cracking activities of zirconia/alumina and alumina may originate from similar hydroxyl species.

The chromia/zirconia catalyst was the most active catalyst in the dehydrogenation of isobutane. Zirconia deposition did not enhance the activity of the chromia/alumina catalysts in the dehydrogenation reaction. Although the Lewis acidity of the support was important for the dehydrogenation performance of the bare supports, no direct correlation was found between the acid–base properties of the supports and the dehydrogenation performance of the chromia catalysts. The higher activity of chromia/zirconia may originate form more easily available chromium species or from a beneficial interaction between the zirconia support and the chromium species. The lower electronegativity of zirconia than of alumina could be the source of such a beneficial interaction. It is suggested that the Cr–O–support bonds are more basic on zirconia than on alumina, and are, therefore, more capable of activating the C–H bonds of isobutane.

It was concluded that even for the zirconia/alumina-supported catalyst with the highest zirconia surface density (5.2 at_{Zr}/nm^2), the zirconia was unable to fully cover the alumina surface, allowing the chromium species to interact with both the zirconia and the alumina. The incomplete monolayer of zirconia and the strong interaction between zirconia and alumina were presumed to cause the lower activity of the zirconia/alumina-supported catalysts. Enhancement of the activity of a zirconia/alumina-supported catalyst would require higher surface densities of zirconia to fully cover the alumina surface and to prevent the interaction. However, the specific surface area of such a catalyst would be lower than the surface areas of the present zirconia/alumina-supported catalysts owing to the gradual formation of crystalline zirconia. Thus, a good course for further research would be to investigate the preparation of pure zirconia with a higher surface area.

7 REFERENCES

1. Eramo, M., Ethylene, Propylene Demand Will Experience Increased Growth in 2005-10, *Oil & Gas J.* **103** (2005) No 45, 52–60.

2. Anon., Western European Market Review, Propylene Production, Consumption and Trade Balance, *Appe, Association of Petrochemicals Producers in Europe*, http://www.petrochemistry.net/statistics-western-european-market-review.html, May 12, 2008.

3. Beury, S., CMAI Completes 2008 World Light Olefin Analysis, *CMAI News* November 15, 2007, http://www.cmaiglobal.com/marketing//News/WLOA2008.pdf, May 12, 2008.

4. Airaksinen, S., *Chromium Oxide Catalysts in the Dehydrogenation of Alkanes*, Doctoral Thesis, Helsinki University of Technology, Espoo, 2005, 58 p.

5. Bhasin, M. M., McCain, J. H., Vora, B. V., Imai, T., Pujadó, P. R., Dehydrogenation and Oxydehydrogenation of Paraffins to Olefins, *Appl. Catal. A* **221** (2001) 397–419.

6. Weckhuysen, B. M., Schoonheydt, R. A., Alkane Dehydrogenation over Supported Chromium Oxide Catalysts, *Catal. Today* **51** (1999) 223–232.

7. Sanfilippo, D., Miracca, I., Dehydrogenation of Paraffins: Synenergies Between Catalyst Design and Reactor Engineering, *Catal. Today* **111** (2006) 133–139.

8. Aittamaa, J., Keskinen, K. I., Flowbat, Neste Oy, Porvoo, 1999.

9. De Rossi, S., Casaletto, M. P., Ferraris, G., Cimino, A., Minelli, G., Chromia/Zirconia Catalysts with Cr Content Exceeding the Monolayer. A Comparison with Chromia/Alumina and Chromia/Silica for Isobutane Dehydrogenation, *Appl. Catal. A* **167** (1998) 257–270.

10. Damyanova, S., Grange, P., Delmon, B., Surface Characterization of Zirconia-Coated Alumina and Silica Carriers, *J. Catal.* **168** (1997) 421–430.

11. Kytökivi, A., Lakomaa, E.-L., Root, A., Österholm, H., Jacobs, J. P., Brongersma, H. H., Sequential Saturating Reactions of $ZrCl_4$ and H_2O Vapors in the Modification of Silica and γ-Alumina with ZrO_2, *Langmuir* **13** (1997) 2717–2725.

12. Jensen, F., *Introduction to Computational Chemistry*, 2nd Edition, John Wiley & Sons, Ltd, Great Britain 2007, pp. 232–267.

13. Sousa, S. F., Fernandes, P. A., Ramos, M. J., Review Article: General Performance of Density Functionals, *J. Phys. Chem. A* **111** (2007) 10439–10452.

14. Menconi, G., Tozer, D. J., Diatomic Bond Lengths and Vibrational Frequencies: Assessment of Recently Developed Exchange-Correlation Functionals, *Chem. Phys. Lett.* **360** (2002) 38–46.

15. Kresse, G., Hafner, J., *Ab initio* Molecular Dynamics for Liquid Metals, *Phys. Rev. B* **47** (1993) 558–561.

16. Kresse, G., Hafner, J., *Ab initio* Molecular-Dynamics Simulation of the Liquid-Metal-Amorphous-Semiconductor Transition in Germanium, *Phys. Rev. B* **49** (1994) 14251–14269.

17. Kresse, G., Furthmüller, J., Efficient Iterative Schemes for *ab initio* Total-Energy Calculations Using Plane-Wave Basis Set, *Phys. Rev. B* **54** (1996) 11169–11186.

18. Kresse, G., Furthmüller, J., VASP the Guide, *http://cms.mpi.univie.ac.at/vasp/vasp/vasp.html*, March 6, 2008.

19. Blöchl, P. E., Projector Augmented-Wave Method, *Phys. Rev. B* **50** (1994) 17953–17979.

20. Kresse, G., Hafner, J., Norm-Conserving and Ultrasoft Pseudopotentials for First-Row and Transition Elements, *J. Phys.: Condens. Matter* **6** (1994) 8245–8257.

21. Kresse, G., Joubert, D., From Ultrasoft Pseudopotentials to the Projector Augemented-Wave Method, *Phys. Rev. B* **59** (1999) 1758–1775.

22. Digne, M., Sautet, P., Raybaud, P., Euzen, P., Toulhoat, H., Priority Communication: Hydroxyl Groups on γ-Alumina Surfaces: A DFT Study, *J. Catal.* **211** (2002) 1–5.

23. Digne, M., Sautet, P., Raybaud, P., Euzen, P., Toulhoat, H., Use of DFT to Achieve a Rational Understanding of Acid-Base Properties of γ-Alumina Surfaces, *J. Catal.* **226** (2004) 54–68.

24. Raybaud, P., Costa, D., Corral Valero, M., Arrouvel, C., Digne, M., Sautet, P., Toulhoat, H., First Principle Surface Thermodynamics of Industrial Supported Catalysts in Working Conditions, *J. Phys.: Condens. Matter* **20** (2008) 064235-1–064235-11.

25. Mukhopadhyay, A. B., Sanz, J. F., Musgrave, C. B., First-Principles Investigation of Hydroxylated Monoclinic HfO_2 Surfaces, *Chem. Matter* **18** (2006) 3397–3403.

26. Hofmann, A., Sauer, J., Surface Structure of Hydroxylated and Sulfated Zirconia. A Periodic Density-Functional Study, *J. Phys. Chem. B* **108** (2004) 14652–14662.

27. Eichler, A., Kresse, G., First-Principles Calculations for the Surface Termination of Pure and Yttria-Doped Zirconia Surfaces, *Phys. Rev. B* **69** (2004) 045402-1–045402-17.

28. Henkelman, G., Uberuaga, B. P., Jónsson, H., A Climbing Image Nudged Elastic Band Method for Finding Saddle Points and Minimum Energy Paths, *J. Chem. Phys.* **113** (2000) 9901–9904.

29. Hafner, J., Adsorption and Reaction of Organic Molecules on Solid Surfaces – *ab-*

initio Density Functional Investigations, *Monatsh. Chem.* **139** (2008) 373–387.

30. Christensen, C. H., Nørskov, J. K., A Molecular View of Heterogeneous Catalysis, *J. Chem. Phys.* **128** (2008) 182503-1–182503-8.

31. Pacchioni, G., Modeling Doped and Defective Oxides in Catalysis with density Functional Theory Methods: Room for Improvements, *J. Chem. Phys.* **128** (2008) 182505-1–182505-10.

32. Thomas, J. M., Heterogeneous Catalysis: Enigmas, Illusions, Challenges, Realities, and Emergent Strategies of Design, *J. Chem. Phys.* **128** (2008) 182502-1–182502-19.

33. Stair, P. C., Advanced Synthesis for Advancing Heterogeneous Catalysis, *J. Chem. Phys.* **128** (2008) 182507-1–182507-4.

34. Weckhuysen, B. M., Wachs, I. E., Schoonheydt, R. A., Surface Chemistry and Spectroscopy of Chromium in Inorganic Oxides, *Chem. Rev.* **96** (1996) 3327–3349.

35. Vuurman, M. A., Wachs, I. E., Stufkens, D. J., Oskam, A., Characterization of Chromium Oxide on Al_2O_3, ZrO_2, TiO_2, and SiO_2 under Dehydrated Conditions, *J. Mol. Catal.* **80** (1993) 209–227.

36. Cherian, M., Rao, M. S., Yang, W.-T., Jehng, J.-M., Hirt, A. M., Deo, G., Oxidative Dehydrogenation of Propane over Cr_2O_3/Al_2O_3 and Cr_2O_3 Catalysts: Effects of Loading, Precursor and Surface Area, *Appl. Catal. A* **233** (2002) 21–33.

37. Puurunen, R. L., Weckhuysen, B. M., Spectroscopic Study on the Irreversible Deactivation of Chromia/Alumina Dehydrogenation Catalysts, *J. Catal.* **210** (2002) 418–430.

38. Hakuli, A., Kytökivi, A., Krause, A. O. I., Dehydrogenation of i-Butane on CrO_x/Al_2O_3 Catalysts Prepared by ALE and Impregnation Techniques, *Appl. Catal. A* **190** (2000) 219–232.

39. Cavani, F., Koutyrev, M., Trifirò, F., Bertolini, A., Ghisletti, D., Iezzi, R., Santucci, A., Del Piero, G., Chemical and Physical Characterization of Alumina-Supported Chromia-Based Catalysts and Their Activity in Dehydrogenation of Isobutane, *J. Catal.* **158** (1996) 236–250.

40. Faro, A. C., Jr., Souza, K. R., Camorim, V. L. D. L., Cardoso, M. B., Zirconia-Alumina Mixing in Alumina-Supported Zirconia Prepared by Impregnation with Solutions of Zirconium Acetylacetonate, *Phys. Chem. Chem. Phys.* **5** (2003) 1932–1940.

41. Faro, A. C., Jr., Souza, K. R., Eon, J. G., Leitão, A. A., Rocha, A. B., Capaz, R. B., Mixed-Oxide Formation During Preparation of Alumina-Supported Zirconia: An EXAFS and DFT Study, *Phys. Chem. Chem. Phys.* **5** (2003) 3811–3817.

42. Gaspar, A. B., Dieguez, L. C., Distribution of Chromium Species in Catalysts Supported on ZrO_2/Al_2O_3 and Performance in Dehydrogenation, *J. Catal.* **220** (2003) 309–316.

43. Burch, R., Loader, P. K., An Investigation of the Use of Zirconia as a Support for Rhodium Catalysts, *Appl. Catal. A* **143** (1996) 317–335.

44. Puurunen, R. L., Formation of Metal Oxide Particles in Atomic Layer Deposition During the Chemisorption of Metal Chlorides: A Review, *Chem. Vap. Deposition* **11** (2005) 79–90.

45. Fernández-García, M., Martínez-Arias, A., Hansom, J. C., Rodriguez, J. A., Nanostructured Oxides in Chemistry: Characterization and Properties, *Chem. Rev.* **104** (2004) 4063–4104.

46. Jomard, G., Petit, T., Pasturel, A., Magaud, L., Kresse, G., Hafner, J., First-Principles Calculations to Describe Zirconia Pseudopolymorphs, *Phys. Rev. B* **59** (1999) 4044–4052.

47. Christensen, A., Carter, E. A., First-Principles Study of the Surfaces of Zirconia, *Phys. Rev. B* **58** (1998) 8050–8064.

48. Hofmann, A., Clarks, S. J., Opple, M., Hahndorf, I., Hydrogen Adsorption on the Tetragonal ZrO_2(101) Surface: A Theoretical Study of an Important Catalytic Reactant, *Phys. Chem. Chem. Phys.* **4** (2002) 3500–3508.

49. Bachiller-Baeza, B., Rodriguez-Ramos, I., Guerrero-Ruiz, A., Interaction of Carbon Dioxide with the Surface of Zirconia Polymorphs, *Langmuir* **14** (1998) 3556–3564.

50. Jung, K. T., Bell, A. T., The Effects of Synthesis and Pretreatment Conditions on the Bulk Structure and Surface Properties of Zirconia, *J. Mol. Catal. A* **163** (2000) 27–42.

51. Morterra, C., Magnacca, G., A Case Study: Surface Chemistry and Surface Structure of Catalytic Aluminas, as Studied by Vibrational Spectroscopy of Adsorbed Species, *Catal. Today* **27** (1996) 497–532.

52. Weckhuysen, B. M., Jehng, J.-M., Wachs, I. E., In Situ Raman Spectroscopy of Supported Transition Metal Oxide Catalysts: $^{18}O_2$–$^{16}O_2$ Isotopic Labeling Studies, *J. Phys. Chem. B* **104** (2000) 7382–7387.

53. Cimino, A., Cordischi, D., Febbraro, S., Gazzoli, D., Indovina, V., Occhiuzzi, M., Valigi, M., Boccuzzi, F., Chiorino, A., Ghiotti, G., The Nature of Surface Chromium Species on CrO_x/ZrO_2 Catalysts, *J. Mol. Catal.* **55** (1989) 23–33.

54. Bañares, M. A., Wachs, I. E., Molecular Structures of Supported Metal Oxide Catalysts under Different Environments, *J. Raman Spectrosc.* **33** (2002) 259–380.

55. Busca, G., The Use of Vibrational Spectroscopies in Studies of Heterogeneous Catalysis by Metal Oxides: an Introduction, *Catal. Today* **27** (1996) 323–352.

56. Groppo, E., Lamberti, C., Bordiga, S., Spoto, G., Zecchina, A., The Structure of

Active Centers and the Ethylene Polymerization Mechanism on the Cr/SiO_2 Catalyst: A Frontier for the Characterization Methods, *Chem. Rev.* **105** (2005) 115–183.

57. Rauhut, G., Pulay, P., Transferable Scaling Factors for Density Functional Derived Vibrational Force Fields, *J. Phys. Chem.* **99** (1995) 3093–3100.

58. Scott, A. P., Radom, L., Harmonic Vibrational Frequencies: An Evaluation of Hartee–Fock, Møller–Plesset, Quadratic Configuration Interaction, Density Functional Theory, and Semiempirical Scale Factors, *J. Chem. Phys.* **100** (1996) 16502–16513.

59. Raybaud, P., Digne, M., Iftimie, R., Wellens, W., Euzen, P., Toulhoat, H., Morphology and Surface Properties of Boehmite (χ-AlOOH): A Density Functional Theory Study, *J. Catal.* **201** (2001) 236–246.

60. Günzler, H., Gremlich, H.-U., *IR Spectrocopy, An Introduction*, Wiley-VCH Verlag GmbH, Federal Republic of Germany 2002, pp. 17–27.

61. Haukka, S., Determination of Chromium in Catalysts by Ultraviolet/Visible Spectrophotometry, *Analyst* **116** (1991) 1055–1057.

62. Rhodes, M. D., Bell, A. T., The Effect of Zirconia Morphology on Methanol Synthesis from CO and H_2 over Cu/ZrO_2 Catalysts, Part I. Steady-State Studies, *J. Catal.* **233** (2005) 198–209.

63. Briand, L. E., Hirt, A. H., Wachs, I. E., Quantitative Determination of the Number of Surface Active Sites and the Turnover Frequencies for Methanol Oxidation over Metal Oxide Catalysts: Application to Bulk Metal Molybdates and Pure Metal Oxide Catalysts, *J. Catal.* **202** (2001) 268–278.

64. Wang, X., Wachs, I. E., Designing the Activity/Selectivity of Surface Acidic, Basic and Redox Active Sites in the Supported K_2O-V_2O_5/Al_2O_3 Catalytic System, *Catal. Today* **96** (2004) 211–222.

65. Guerrero-Pérez, M. O., Bañares, M. A., From Conventional in Situ to Operando Studies in Raman Spectroscopy, *Catal. Today* **113** (2006) 48–57.

66. Rao, T. V. M., Deo, G., Jehng, J.-M., Wachs, I. E., In Situ UV-Vis-NIR Diffuse Reflectance Raman Spectroscopy and Catalytic Activity Studies of Propane Oxidative Dehydrogenation over Supported CrO_3/ZrO_2 Catalysts, *Langmuir* **20** (2004) 7159–7165.

67. Iskandarova, I. M., Knizhnik, A. A., Rykova, E. A., Bagatur´yants, A. A., Potapkin, B. V., Korkin, A. A., First-principle Investigation of the Hydroxylation of Zirconia and Hafnia Surfaces, *Microelectron. Eng.* **69** (2003) 587–593.

68. Ignatchenko, A., Nealon, D. G., Dushane, R., Humphries, K., Interaction of Water with Titania and Zirconia Surfaces, *J. Mol. Catal. A* **256** (2006) 57–74.

69. Ouyang, F., Kondo, J. N., Maruya, K., Domen, K., IR Study on H/D Isotope Exchange Reaction of Formate and Methoxy Species with D_2 on Zirconia, *J. Chem. Soc., Faraday Trans.* **93** (1997) 169–174.

70. Busca, G., Lamotte, J., Lavalley, J.-C., Lorenzelli, V., FT-IR Study of the Adsorption and Transformation of Formaldehyde on Oxide Surfaces, *J. Am. Chem. Soc.* **109** (1987) 5197–5202.

71. Finocchio, E., Busca, G., Lorenzelli, V., Willey, R. J., FTIR Studies on the Selective Oxidation and Combustion of Light Hydrocarbons at Metal Oxide Surfaces, Propane and Propene Oxidation on $MgCr_2O_4$, *J. Am. Chem. Soc., Faraday Trans.* **90** (1994) 3347–3356.

72. Finocchio, E., Busca, G., Lorenzelli, V., Willey, R. J., The Activation of Hydrocarbon C–H Bonds over Transition Metal Oxide Catalysts: A FTIR Study of Hydrocarbon Catalytic Combustion over $MgCr_2O_4$, *J. Catal.* **151** (1995) 204–215.

73. Dilara, P. A., Vohs, J. M., TPD and HREELS Investigation of the Reaction of Formic Acid on ZrO_2(100), *J. Phys. Chem.* **97** (1993) 12919–12923.

74. Persson, P., Ojamäe, L., Periodic Hartee-Fock Study of the Adsorption of Formic Acid on ZnO($10\bar{1}0$), *Chem. **Phys**. Lett.* **321** (2000) 302–308.

75. Bates, S. P., Kresse, G., Gillan, M. J., The Adsorption and Dissociation of ROH Molecules on TiO_2(110), *Surf. Sci.* **409** (1998) 336–349.

76. Collins, S. E., Baltanás, M. A., Bonivardi, A. L., Mechanism of the Decomposition of Adsorbed Methanol over Pd/α,β-Ga_2O_3 Catalyst, *Appl. Catal. A* **295** (2005) 126–133.

77. Fisher, I. A., Bell, A. T., A Mechanistic Study of Methanol Decomposition over Cu/SiO_2, ZrO_2/SiO_2, and Cu/ZrO_2/SiO_2, *J. Catal.* **184** (1999) 357–376.

78. Ricote, S., Jacobs, G., Milling, M., Ji, Y., Patterson, P. M., Davis, B. H., Low Temperature Water-Gas Shift: Characterization and Testing of Binary Mixed Oxides of Ceria and Zirconia Promoted with Pt, *Appl. Catal. A* **303** (2006) 35–47.

79. Ermini, V., Finocchio, E., Sechi, S., Busca, G., Rossini, S., An FT-IR and Flow Reactor Study of the Conversion of Propane on γ-Al_2O_3 in Oxygen-Containing Atmosphere, *Appl. Catal A* **190** (2000) 157–167.

80. Pater, J., Cordona, F., Canaff, C., Gnep, N. S., Szabo, G., Guisnet, M., Alkylation of Isobutene with 2-Butene over a HFAU Zeolite. Composition of Coke and Deactivating Effect, *Ind. Eng. Chem. Res.* **38** (1999) 3822–3829.

81. Kuba, S., Knözinger, H., Time-Resolved in Situ Raman Spectroscopy of Working Catalysts: Sulfated and Tungstated Zirconia, *J. Raman Spectrosc.* **33** (2002) 325–332.

ISBN 978-951-22-9551-7
ISBN 978-951-22-9552-4 (PDF)
ISSN 1795-2239
ISSN 1795-4584 (PDF)